Experimental Analysis and Theoretical Modeling of Forced Mechanical Response of Nitinol Stent for Popliteal Segment of Femoral Region

A THESIS SUBMITTED TO THE GRADUATE DIVISION OF THE UNIVERSITY OF HAWAIʻI AT MANOA IN PARTIAL FULFILLMENT OF THE REQUIREMENTS FOR THE DEGREE OF

MASTER OF SCIENCE

IN

MECHANICAL ENGINEERING

AUGUST 2012

By
Atma Bhawuk

Thesis Committee:

Dr. Scott Miller, Chairperson
Dr. Marcelo Kobayashi
Dr. Olga Boric-Lubecke

We certify that we have read this thesis and that, in our opinion, it is satisfactory in scope and quality as a thesis for the degree of Master of Science in Mechanical engineering.

THESIS COMMITTEE

_____

Chairperson

_____

_____

Acknowledgements

I would like to thank my family and friends for their support in this endeavor. In particular, I would like to recognize my father, mother, and brother, without whose indelible examples, I am sure, I would have easily forgotten that "life is a marathon," and "one who runs, wins the race." I would also like to thank Dr. Marcelo Kobayashi and Dr. Olga Boric-Lubecke for providing me with guidance in coursework and this project. My involvement in their courses has helped mold my interests, cultivate my strengths, and bolster my weaknesses. Finally, I would like to express heartfelt thanks to Dr. Scott Miller for his support, patience, and mentorship. There is no conceivable way I would be in this position without your guidance. Working with you has been a wonderful and rewarding learning experience that I will continue to cherish. Thank you.

Abstract

Stents are small, wire-mesh struts that are placed into arteries after an angioplasty procedure. The purpose of a stent is to help keep the portion of the blood vessel that has been treated with angioplasty open after the procedure. Stents have been used to help substantially reduce the restenosis associated with angioplasty procedures. Two broad categories of stents are self-expanding and balloon expanding. Balloon expandable stents have been available for several years, but the application of shape memory alloys to the manufacture of stents is relatively new. The differences between the two stents stem mainly from the material of construction. Self-expanding stents are investigated in this study. In particular, the mechanical response of a bare stent made of a shape memory alloy (SMA), Nitinol is investigated here.

The Nitinol stent is investigated experimentally and using finite element methodology (FEM). The Guidant Absolute Nitinol Stent is experimentally tested for various uniaxial tensile loading conditions. In addition the stent specimen was subject to compressive, and crush loads as well. The stent geometry was rendered using computer aided design (CAD) software, Solidworks. Several different lengths of the stent were created, but only 7.30, 10.87, 14.42 mm stents were subject to the same uniaxial tensile, and compression loads. The crush test was not simulated. In addition three modifications to the Absolute stent geometry were also created and tested for the same uniaxial tensile loads. Results from the simulation were validated against the experimentally acquired results.

Comparison of the simulation and experimental results reveals that the load-strain relationship from the different simulated lengths is similar to that found experimentally. The simulation represented the elastic region of the Nitinol stent under tensile loading well. The experimental results showed a steeper elastic region, which was accounted for by the increased length of the stent. The load-strain curve comparison reveals that the load at which the Nitinol undergoes phase transformation is 0.9 N from experiment and approximately 0.7 N from the simulations. The model correctly predicted the locations of concentrated stress, in turn, accurately identifying the regions that would be expected to suffer structural failure. Moreover, the geometry modifications reveal a dependence of the stiffness of the stent on the number, location, and length of the bridge elements.

Table of Contents

Acknowledgements iv
Abstract v
Nomenclature viii
List of Tables ix
List of Figures x
1 Introduction 1
1.1 Background 1
1.1.1 Stents: An Overview 1
1.1.2 Typical materials in stent design 3
1.1.3 Material Properties of Nitinol 4
1.1.3.1 Martensitic Transformation 4
1.1.3.2 Shape Memory Effect 6
1.3.3.3 Superelasticity 7
1.1.3.4 Elastic Properties 9
1.2 Research Motivation 10
1.3 Literature Review 12
1.3.1 Comparison of BE and SE Stents 12
1.3.2 FEM Modeling of Stent Geometries 13
1.4 Research Issues and Thesis Organization 15
1.4.1 CAD Model Formulation of Commercial SE Stents 15
1.4.2 Comparison of Experimental and Theoretical Results 17
1.4.3 FEM as a Tool for Prediction of Structural Integrity 17
1.4.4 Thesis Organization 18
2 Finite Element Modeling of Stent Behavior 19
2.1 Introduction 19
2.2 Review of Stent Modeling 21
2.3 CAD Model of Stent Geometry 25
2.4 FEM Theory 27
2.4.1 Material Modeling 32
2.4.2 Mechanical Response 39
2.5 Finite Element Simulation 43
2.5.1 FEM Techniques 43
2.5.2 Model parameters and material properties 44
2.6 Investigation of Model Parameters 47
2.7 FEM Analysis of Work-Material Deformation and Stress 53
2.8 Conclusions 54
3 Experimental Analysis of Absolute Stent 56

3.1 Introduction 56
3.2 Literature Review 57
3.3 Stent Property Experimental Measurements 58
3.3.1 Experimental Setup and Procedure 60
3.3.2 Results and Discussion 61
3.3.2.1 Elastic Deformation 61
3.3.2.2 Large Deformation: Tensile Test to Fracture 62
3.4 Conclusions 66
4 Quantification and Comparison of FEM Models to Experimental Results 68
4.1 Introduction 68
4.2 Theoretical Data vs. Experimental Data For Nitinol Absolute Stent 68
4.3 Proposed Design Changes 70
4.3.1 CAD Design 70
4.3.2 Theoretical Results for Modified Geometries 71
4.4 Conclusions 74
5 Conclusions 75
5.1 Summary 75
5.2 Conclusions 75
5.3 Contributions 77
5.4 Future Work 78
6 References 79

Nomenclature

BE: Balloon Expanding
CABG: Coronary Artery Bypass Graft
CAD: Computer Aided Design
FDA: Food and Drug Administrations
FEM: Finite Element Modeling
SE: Self Expanding
SMA: Shapte Memory Alloy
PTCA: Percutaneous Transluminal Coronary Angioplasty
A_f: Austenite finish temperature
M_f: Martensite finish temperature
T_{room}: Room Temperature
E: Young's Modulus
ρ: Density
ν: Poisson's Ratio
ψ: Helmholtz Potential
u: Specific Internal Energy
h: Specific Enthalpy
s: Entropy
σ: Stress
ϵ: Strain
q: heat flux
e^{tr}: Internal state variable (second order traceless tensor)
σ_o: Stress value indicating the mean value of the mechanical hysteresis
σ_s: Stress threshold value at which austenite to martensite transformation begins
ε_L: Maximum transformation strain reached at the end of the austenite to martensite transformation
R: Measure of the mechanical hysteresis amplitude

List of Tables

Table 2.1: Properties of Steel AISI 4340 47

Table 2.2: Properties for Simple Nitinol Model 47

Table 2.3: Properties for Complicated Nitinol Model 49

List of Figures

Fig. 1.1 External Forces Acting on Artery 3
Fig. 1.2 2-D Transformation from austenite to martensite 5
Fig. 1.3 Deformation of Nitinol, and Nitinol Stress-Strain 7
Fig. 1.4 Stress-Strain-Temperature for SMA 9
Fig. 1.5 Stress-hysteresis and biased stiffness 10
Fig. 2.1 CAD Model of Absolute stent 26
Fig. 2.2 CAD Model – Three Lengths 27
Fig. 2.3 Pseudoelastic Effect 39
Fig. 2.4 Constraints and Load 44
Fig. 2.5 Mesh of Absolute Stent 45
Fig. 2.6 Mesh Sensitivity 46
Fig. 2.7 Tensile Loadings for 7.30 mm and 10.87 (simple Nitinol) 48
Fig. 2.8 Load-Strain 7.30 mm 50
Fig. 2.9 Stress-Strain for all 3 Lengths 51
Fig. 2.10 Load-Strain 10.87 mm 52
Fig. 2.11 Load-Strain 14.42 mm 52
Fig. 2.12 Comparison of theoretical Load-Strain 53
Fig. 2.13 von Mises for 10.87 (simple Nitinol) 53
Fig. 2.14 von Mises for 3 stent lengths (complicated Nitinol) 54
Fig. 3.1 Tension device for Nitinol stent 57
Fig. 3.2 Experimental setup for crush test 59
Fig. 3.3 INSTRON materials tester and stent on graspable adapter 60
Fig. 3.4 GUIDANT stent under loading conditions 61
Fig. 3.5 Experimental Load-Strain 62
Fig. 3.6 Deformed Absolute Stent 64
Fig. 3.7 Tension Test till Fracture 64
Fig. 3.8 Contraction Test 65
Fig. 3.9 Crush Test 66
Fig. 4.1 Experiment and basic Nitinol model 69
Fig. 4.2 Experiment and complicated Nitinol model 70
Fig. 4.3 Elastic region comparison 70
Fig. 4.4 CAD modified stent geometries 71
Fig. 4.5 7.30 and 10.87 mm stents with MOD 1 72
Fig. 4.6 Comparison of MOD 1to actual stent theoretical 72
Fig. 4.7 Comparison of MOD 2 to actual stent theoretical MOD 1 73

Chapter 1: Introduction

1.1 Background

1.1.1 Stents: An Overview

Stents are small, wire-mesh struts that are placed into arteries after an angioplasty procedure. The purpose of a stent is to help keep the portion of the blood vessel that has been treated with angioplasty open after the procedure. Stents have been used to help substantially reduce the restenosis associated with angioplasty procedures. Two broad categories of stents are bare metal and drug eluting stents. Drug eluting stents are a more recent development and are coated with drugs to limit the tissue growth that leads to restenosis. Stents come in numerous sizes and shapes, which afford medical practitioners choices that will best fit the patients' artery.

A *vascular stent* is a "synthetic tubular structure that is permanently implanted in the native or grafted vasculature and that is intended to provide mechanical and radial support to enhance vessel patency" [ASTM, 2009]. For the purposes of this study vascular stents are assumed to be metallic alloys. S*E* stents are defined as "as stent that expands without extrinsic force or pressure, to a size and shape close to the desired final size and shape, when released from the delivery system. The self-expanding nature of stents is a design feature resulting from the materials of construction or the structural geometry, or both" [ASTM, 2009]. Generally cylindrical in shape, SE stents are composed of a finite number of linkages referred to as *bridges*. These *bridges* are connecting elements between the radial support aspects of the stent [ASTM, 2009]. A bridge may have unique design features, as compared to a strut, to enhance longitudinal flexibility and minimize shortening. A *strut* is "the smallest individual element of the radial support aspect of a stent that has solid cross section in both the radial and circumferential directions" [ASTM, 2009]. The *diameter* refers to the inner diameter of the stent (ID), unless otherwise specified. To *crimp* a stent means to secure it to the delivery system by compressing the stent onto a balloon, and they may be obtained in an un-mounted or pre-mounted fashion.

The first implanted stent was described by Dotter [1969] to treat arterial shrinkage. Since 1969 stents have been pursued as a supplement or alternative to conventional balloon angioplasty for arterial occlusive diseases [Duda et al., 2000]. Although, the first clinical implantations began in the early 1990s, several stent designs have been developed. As with any structure physical properties play a key role in the structural performance. Material considerations

become important and the material must, not only, be biocompatible but also suitable to handle the mechanical stresses in the region of the lesion. Thus, the stent is an artificial tube inserted into the natural conduits of the body in order to prevent or counteract a disease-induced localized flow constriction. Although the stent can be considered as a tool used to keep the vessel of interest open during surgery.

The most widely known stents are of the bare-metal, drug-eluting, or covered variety for use in the coronary arteries (angioplasty). Stents, however, can also be used in a wide variety of bio-conduits. Other examples include ureteral stents, which are used to ensure the patency of the ureter that may be compromised due to a kidney stone. In some cases ureteral stents are used as a preliminary measure to prevent blockage until surgery can be performed to remove the stone. Furthermore, a prostatic stent can be used to aid men who have trouble urinating. Moreover, stents may be ideal components for peripheral arterial angioplasty; these are due to atherosclerotic narrowing in the leg, abdomen, or renal arteries. Esophageal stents also diversify the already numerous uses of medical stents.

Intravascular stents are small tube-like structures that are commonly used to open arteries that have become clogged due to the build-up of fat, cholesterol, and other substances over time [Migliavacca et al., 2002]. Stents were used as an alternative to offset disadvantages of balloon angioplasties, such as restenosis and abrupt closure [Dangas and Fuster, 1996]. A higher efficiency of stents is supported by randomized clinical trials and clinical studies [Fischmann et al., 1994], but problems related to migrations, collapses, positioning difficulties, material considerations pose new issues in the development of stents and associated procedures. Different typologies of stents are available in the market and it behooves the operator to know the different physical properties of the stent selected to treat a specific lesion [Magliavacca et al., 2002].

Stenting the atherosclerotic lesions in the femoral and popliteal arteries can still be a very complicated procedure. Complications arise due to the unique forces and deformations a stent segment experiences in this region. As such, commercial stents for this region of the body are not readily available and need to be developed to advance endeavors to successfully treat health risks and issues associated with the peripheral arterial system. The femoropopliteal region is very dynamic and experiences high, repetitive mechanical stresses. With knee flexion and interactions with surrounding musculature, this arterial segment is exposed to large angle

changes and a variety of external forces, including extension/contraction, torsion, compression, torsion, and bending (Fig. 1) [3, 5]. Such mechanical forces can also translate to clinical consequences when a stent is placed in the femoropopliteal segment. Stent compression has been identified as one of the principal causes of restenosis [3], and the mechanical bending due to knee joint flexion can limit long-term patency of stents [2]. Therefore, stents placed in the femoropopliteal region must be designed with longitudinal elasticity, and capabilities to withstand torsional, bending, and compression stresses.

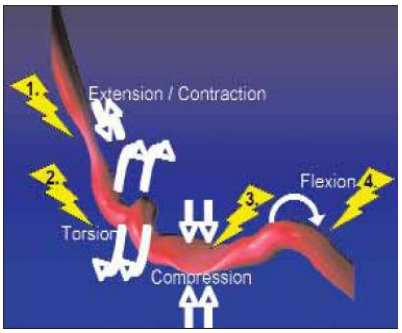

Fig. 1.1 External forces acting on the femoropopliteal artery.

1.1.2. Typical Materials in Stent Design

There is growing interest in the use of nickel-titanium alloys (Nitinol) for the framework of stents. Nitinol, developed on the Naval Ordnances Laboratory, is a superelastic, shape memory alloy. The alloy is generally comprised of 55% nickel, and 45% titanium and has the ability to return to a specific shape upon heating or cooling to a certain temperature after its phase transition. The strong inter-metallic bonds between nickel and titanium have a low reaction rate, even in patients with increased sensitivity to nickel [Lim, 2004]. This leads to a strong immunological response and prevents corrosion. Although it is difficult to manufacture, the shape memory and biocompatibility of this material make it a highly desirable material for use in the manufacture of stents. Since titanium is highly reactive with oxygen and nitrogen particles in the air, the manufacturing costs of this material limit the proportion of stents made from it; currently only 5% of stents are made from Nitinol [Lim, 2004]. Furthermore, areas such as the femoral popliteal artery that experience unique mechanical stresses could use the superelastic property of this material to create more feasible stenting options.

As with any other structure, the physical properties of the stent material are paramount. The material used to create stents must be flexible, supportive, capable of expansion, and

biocompatible [Lim, 2004]. A biocompatible material is one that does not induce a toxic or detrimental immunological response in the patient. The ability of a material to perform with an appropriate host response in a particular application forms the crux of biocompatibility [Lim, 2004] and leads to the consideration of some materials over others.

Currently, most scaffolding of bio-conduits is done using a stainless steel. However, stent framework created from 316L stainless steel is not entirely biocompatible and leads to complications such as restenosis and thrombosis. Examples of these stents include the Cordis Palmaz-Schatz stent, the Cordis Crossflext stent, the Guidant MultiLink stent, and the Medtronic Bestent [Lim, 2004]. Although these stents are functional and commercially available, there are several drawbacks that foster the need for the development of new materials that increase the biocompatibility of the stent. In particular, shortcomings of the 316 stainless steel stents can be in seen in a high occurrence of subacute thrombosis and restenosis, percutaneous bleeding, corrosion, and re-dilation of the stented vessel segment [Lim, 2004]. Furthermore, the radiopacity or viewing capacity of stainless steel stents can also be improved.

Gold can be used to improve the visibility of 316L stainless steel stents; it is a highly, visible, biocompatible, and inert metal. Although gold plated hybrid stents offer good flexibility and visibility, their manufacturing costs are high. Several alloys have also been considered in the design and manufacture of stents. For example, cobalt-chromium-nickel-molybdenum-iron, first used to make watch springs is now used in the Schneider Wallstent. Tantalum is a material that is more brittle than stainless steel but provides higher ductility and resistance to corrosion, and is used in stents like the Wiktor Stent by Medtronic, and the Tantalum Cordis Stent [Lim, 2004].

1.1.3. Material Properties of Nitinol

1.1.3.1. Martensitic Transformation

Solid state transformations are generally of two types: diffusional and displacive. Diffusional transformations involve the random motion of atoms over relatively long distances. In this type of transformation the long range diffusion is required because the new phase is of a different chemical composition than the original matrix from which it was formed [Duerig, 1990]. Since atomic migration is the key to this type of solid state, it is both time and temperature dependent. In contrast, displacive transformations do not require long range movement of atoms [Duerig, 1990]. Atoms are cooperatively rearranged into a more stable

crystal lattice, without change to the chemical nature of the matrix. Since atomic migrations are not necessary in this type of transformation, they are usually time-independent [Duerig, 1990]. Martensitic transformations are usually of this type, and are formed by cooling the higher temperature parent, or austenite phase.

Martensitic formation is a first order transformation that releases heat. Moreover, there is a hysteresis associated with the transformation suggesting that there is a temperature range over which martensite and austenite co-exist [Duerig, 1990]. Thus, martensite is formed when cooling from the parent phase with the volume fraction of martensite increasing independent of time. Crystallographically, the transformation from austenite to martensite can be thought of in two parts [Duerig, 1990]. The Bain strain (Fig. 2(a)) or lattice deformation incorporates all the atomic movements needed to produce the new structure from the old.

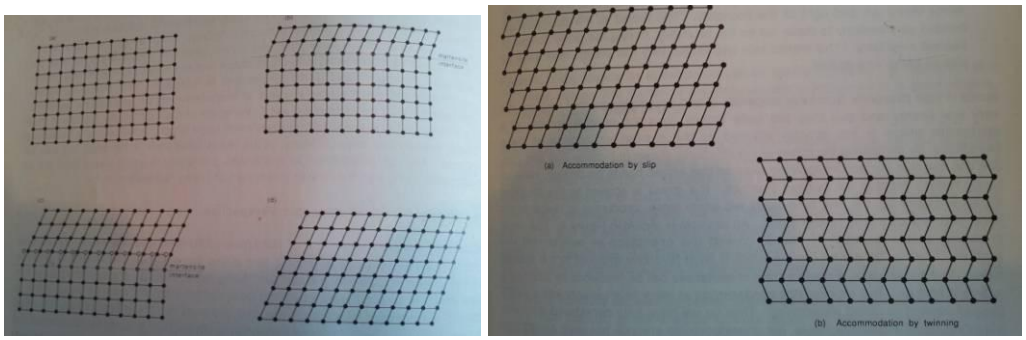

(a) (b)

Fig. 1.2. (a) Transformation from austenite to martensite in two dimensions and (b) two mechanisms for accommodating shape change due to atomic shear of Martensitic transformation [Duerig, 1990]

In Fig. 2(a), the austenite structure is presented in the upper left hand corner and the progression is illustrated schematically in two dimensions to show that as the interface progresses one atomic layer, each atom is only required to move only a very small amount [Duerig, 1990]. The final result of these movements is the formation of the Martensitic structure and the movements resulting in said structure are referred to as the Bain strain [Duerig, 1990]. It is important to note, however, that a two-dimensional representation of Bain strain does not take into account the several atomic shuffles that are necessary in addition to the movement illustrated in Fig. 2(a).

The second part of the Martensitic transformation is the lattice invariant shear, an accommodation step. Since the Martensitic structure formed by the Bain strain is of a different

shape, and volume than the surrounding austenite. Martensite in steel involves a volume and a shape change, but martensite formation in shape memory alloys such as NiTi, involves only a shape change [Duerig, 1990]. Therefore, the shape of the new phase or the shape of the surrounding austenite must be changed in order to accommodate the new shape. Two general mechanisms associated with this accommodating step are slip and twinning, as shown in Fig. 2(b). Slip is a process, in which the microstructure is permanently changed. Twinning can accommodate shape changes in a reversible way but cannot do the same for changes in volume. In order for the shape memory effect to be applicable the accommodation step must be completely reversible, indicating that twinning must be the dominant accommodation mechanism. Thus, twinning process of accommodation plays a key role in the shape memory effect [Duering, 1990].

1.1.3.2. Shape Memory Effect

Shape memory alloys are examples of active materials that are multifunctional, i.e., lighter, stronger materials with tailored properties [Lagoudas, 2008]. These multifunctional materials have sensing and actuation capabilities in that they can take a mechanical signal and convert it to a non-mechanical output, e.g., voltage, or convert a non-mechanical input to a mechanical output. It is important to note that active materials generally have a mechanical response when subjected to a non-mechanical field. Examples of active materials include piezoelectric and electrorestrictive devices, piezomagnetic and magnetorestrictive devices, and shape memory materials.

Shape memory alloys recover shape when the temperature is increased, even under a high load, indicating that they have high actuation densities. They can also absorb and dissipate mechanical energy by undergoing a reversible hysteric shape change when subjected to an applied mechanical cyclic load [Lagoudas, 2008]. Nitinol (NiTi) is one such shape memory alloy and has two distinct characteristics (shape memory and superelasticity) in addition to its biocompatibility that make it a perfectly suitable material for design considerations for implantable stents. The unique material properties of NiTi alloys are well explored with respect to the load and temperature dependent mechanism of the phase transformation from austenite to martensite [Simons et al., 2010] that underlie the superelastic and shape memory responses of the material.

The elastic deformation of conventional stent materials such as stainless steel, and cobalt based alloys are significantly different from the elastic response of structural materials of the living body [Simons et al., 2010]. Whereas the elastic deformation of these conventional materials are approximately 1% strain, those of the natural materials can be up to 10% strain. Moreover, for conventional stent materials the elongation increases and decreases linearly with the applied force, whereas the deformations of natural materials are characteristically non-linear. Upon release of the deformation stress, the strain is recovered at lower stresses, as shown in Fig. 3(a). It becomes evident that the loading and unloading cycle is characterized by a pronounced hysteresis [Stoeckel et al., 2004].

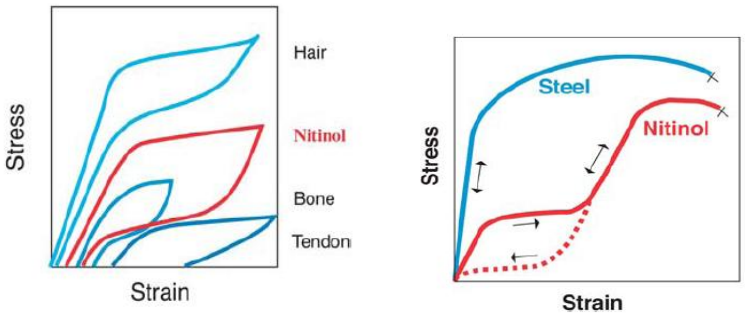

(a) (b)

Fig. 1.3. (a) Deformation characteristics of Nitinol and living tissues and (b) schematic stress-strain diagram for Nitinol and stainless steel

1.1.3.3. Superelasticity

Equiatomic, or near equiatomic, compositions of nickel and titanium, exhibit behaviors similar to those of living tissue. A characteristic stress-strain curve for steel and Nitinol is shown in Fig. 3(b). As evidenced by the figure, the loading and unloading curves for Nitinol are similar to those of natural materials. In addition to showing plateaus similar to natural materials the stress-strain curve also indicates that along these plateaus large deflections (strains) can be accumulated while loading and recovered while unloading [Stoeckel et al., 2004]. These deflections can clearly be accumulated or recovered without significant increase, decrease, respectively in the loads (stress). Since deformations of nearly 10% strain can be elastically recovered, this behavior is called superelasticity.

Superelastic Nitinol appears on a macroscopic level to be “very” elastic. However, it is important to note that the mechanism of deformation is different from conventional elasticity, or the stretching of atomic bonds. When a stress is applied to Nitinol, an elastic deformation occurs

after which material yields to the applied stress by changing its crystal structure [Stoeckel, D. et al., 2004]. This stress induced phase transformation causes the Nitinol to change shape as a direct response to the applied load. Once the stress is removed the material reverts back to its original shape.

Whereas, superelasticity is caused by a stress-induced transformation, the shape memory effect (SME) results due to a thermal phase transformation. When the Nitinol is cooled below a critical temperature (dependent on alloy composition and processing history), an associated change in the crystal structure occurs. If no force is applied this microscopic phase change is not associated with a macroscopic shape change. Thus, the material can be plastically deformed in the low temperature phase but can be restored to the original shape by heating above the transformation temperature [Stoeckel et al., 2004]. The transformation temperature is typically set to 30^{o}C.

SME and superelasticity of the shape memory alloy can be elaborated upon in terms of the martensite and austenite formation temperatures, as shown in Fig. 4. Specifically, the shape memory alloy exhibits SME when it is deformed at M^{t}, the temperature at which all the austenite has transformed into martensite [Lagoudas, 2008]. Once it is unloaded at a temperature less than A^{s} (austenite formation start temperature), and heated back to a temperature greater than A^{t} (austenite formation finish temperature), the shape memory alloy will regain its original shape. The superelastic behavior of shape memory alloys is, therefore, associated with the stress induced transformation which leads to strain generation during the loading phase, and subsequent strain recovery upon unloading at a $T > A^{t}$. The reversible phase transformation caused by the thermo-mechanical loading path refers to the superelastic properties of shape memory alloys like Nitinol. Furthermore, the shape memory alloy can exhibit repeatable shape changes under no applied mechanical load, when subjected to cyclic thermal loading [Lagoudas, 2008]

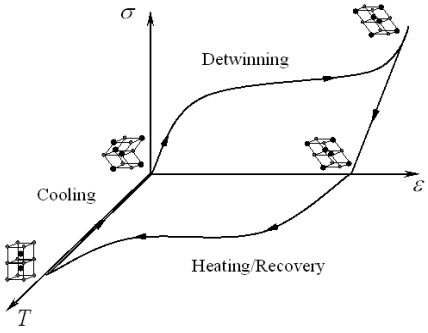

Fig. 1.4. Stress-Strain-Temperature Curve for Shape Memory Alloys to show loading and unloading plateaus

1.1.3.4. Elastic Properties

Nitinol shape memory alloys are among the most studies, and most commercially viable materials for the design and manufacture of biological stents. They exhibit the aforementioned SME, and superelasticity, and significant resistant to corrosion to provide more than adequate biocompatibility [Lagoudas, 2008].

Nitinol is an alloy generally composed of 55 weight percent nickel and the balance titanium. As mentioned, it has unique properties derived from the solid state transformation triggered either mechanically or thermally [Stoeckel et al., 2004]. In addition to the commonly known material characteristics such as Young's modulus, yield strength, ultimate tensile strength, and elongation to failure, properties such as transformation temperature, upper and lower plateau stress, recoverable strain, and permanent set must be accounted for [Stoeckel et al., 2004].

While considering typical material characteristics, and those characteristic of shape memory alloys, it is important to note that the most unusual property of Nitinol is stress hysteresis. In most materials stress increases linearly with strain upon loading and decreases along the same path upon unloading [Stoeckel et al., 2004]. However, Nitinol is distinctly different. The stress hysteresis or path dependence of the strain loading and unloading is shown in Fig. 5. After an initial linear increase in stress with the strain, large strains can be obtained with only a slight increase in the stress (loading plateau). The end of this plateau is reached at approximately 8% strain. Unloading causes the stress to decrease rapidly, until another plateau is reached, where the strain can be recovered with very little decrease in the stress. This characteristic of Nitinol can be termed biased stiffness (Fig. 5). The same cycle can be used to follow the cycle of crimping a stent into a delivery system, deploying it, and having it expand and interact with the vessel. These are discussed in the relation to Nitinol in section 1.3.2, which is concerned with a

literature review of self-expanding (SE) stents with particular attention focused on stents made of a NiTi alloy.

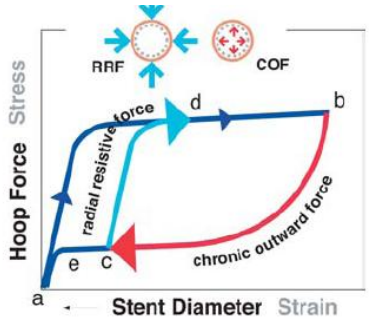

Fig. 1.5. Schematic stress hysteresis and biased stiffness [Stoeckel, D. et al., 2004]

Just as Nitinol requires controlled processing to achieve optimal shape memory and superelastic properties surface processing is required to promote corrosion resistance and biocompatibility. Although not a concern of this study, it is important to note that the corrosion resistance of properly treated Nitinol rivals that of titanium and other common implant materials. As is the case with any implant, the biocompatibility of the material is just as important, if not more so, than other material properties, and is worth mentioning here.

1.2 Research Motivation

There currently is no finite element model (FEM) for Nitinol stents that is useful for predicting the effect of structure and material properties on force response efficiently. For the most part, the structure of the stent has been determined by experimental trial and error methods, which requires costly laser cutting process for each stent design. This is neither cost effective, nor is it an appropriate usage of time and resources. Thus, the need for a FEM to test stents *before* they are manufactured needs to be developed. Such a predictive model would allow researchers and manufacturers to determine the mechanical response of proposed stent designs to various loads. This research specifically focuses on foreshortening, contraction, bending, torsional, and crush loads in the FEM domain. The success of the FEM presented in this research is contingent upon accurate material modeling of the shape memory alloy (SMA) Nitinol, as well as appropriate loading conditions experienced within the body, in particular, those stresses experienced in the femoropopliteal artery (knee). With the development of this FEM, time and resources could be concentrated on practical solutions for the stenting of blood vessels that experience a variety of mechanical stresses within the body.

Despite advances in the treatment of patients with peripheral arterial disease (PAD), the optimal treatment strategy for atherosclerosis in the femoropopliteal segment remains debatable [Ma, 2006]. The most common method for the management of PAD is percutaneous transluminal angioplasty, but the elastic recoil of the expanded vessel leads to restenosis and is a major drawback of the procedure. Stenting of the femoropopliteal artery is a viable solution, but stents have been evidenced to fracture or recoil due to the high mechanical stresses of the region [Ma, 2006]. Thus a more robust stent design for the popliteal segment becomes a necessity.

Over 100 different stent designs are currently being marketed or evaluated for application to vascular and non-vascular indications [Stoeckel et al., 2002]. However, development of fracture resistant stents requires a better understanding of *in-vivo* loads, and how stents deform under these loads, as well, as the influence of the artery on stent deformation. Changes of stent geometry under load, and the deformation, load, and stent artery interaction information is needed to validate finite element models for designing and analyzing stents.

Current stent design is primarily focused with providing adequate radial support to the artery. They are generally tested with respect to fatigue response under pulsatile loads that simulate the cyclic radial expansion of the stent due to the normal blood pressure fluctuation within the body. Very little data is available with regard to the overall structural response of stents to axial, bending, and torsional loads, especially with consideration given to arterial interaction [Simons et al., 2010]. Moreover, there is a significant lack of data associated with stenting the femoropopliteal artery. As this area experiences unique mechanical stresses not experienced in other regions of potential stent implantation, careful attention needs to be paid to the type of stent and its response to the loads experienced in this region.

Thus, the importance of a study that uses the finite element method to model the mechanical response of market available and potential stents for the femoropopliteal region becomes self-evident. As there is insufficient data, such a study would furnish simulation data that would be useful in the comparison of the actual performance of Nitinol stents for the femoropopliteal to simulated models. The validity of these models could then be used to design and manufacture more robust stents that can withstand *in-vivo* loads without compromising their structural integrity.

1.3. Literature Review

This section presents the foundation of the body of literature found for this research. Chapters 2 and Chapter 3 provide more focused literature reviews pertaining to theoretical modeling and experimental setups respectively. The theoretical modeling literature review highlights pertinent journal articles related to the modeling of SMAs and more specifically the modeling of Nitinol. Moreover, the theoretical modeling literature review in chapter 2 explores the modeling of SMAs using COMSOL. The experimental literature review presents experimental studies related to the load deformation behavior of the Nitinol work-material as well as studies involving the fatigue characteristics of Nitinol. The experimental setups cited in chapter 3 are used as a reference for the experimental testing of the Guidant Absolute Stent in this investigation.

1.3.1. Comparison of BE and SE Stents

Stents are manufactured as one of two particular designs. The first is referred to as balloon-expandable (BE) stents, while the other is the SE stents, and is the major focus of this study. There are key differences between the BE and SE stents that include material properties that generally stem from the implantation location. Engineering and design differences between the two different types of stents can be compared to the clinical performances of both in order to make accurate recommendations as to which stents are the most appropriate given a particular implantation scenario. While neither stent can be considered universally superior, the differences are significant enough to make one more appropriate than the other in specific circumstances [Duerig and Wholey, 2002].

BE stents are manufactured in the crimped state and expanded to the vessel diameter using a balloon, thus plastically deforming the stent. On the other hand SE stents are manufactured at the vessel diameter and crimped and constrained at a smaller diameter until the intended delivery site is reached at which point the constraint is removed and the stent is deployed [Duerig and Wholey, 2002]. Thus, BE stents resist the balloon expansion while SE stents assist the vessel expansion. Although BE stents were commercially distributed first, SE stents have captured a significant portion of the peripheral vascular market.

Radial strength describes the external pressure that a stent is able to withstand without incurring any clinically significant damage [Duerig and Wholey, 2002]. One can consider a permanent decrease in the vessel lumen diameter as significant damage. BE stents can collapse

if a critical external pressure is exceeded, resulting in a buckling phenomenon. SE expanding stents on the other hand are superelastic and have no strength limitation and elastically recover even after complete flattening or radial crushing [Duerig and Wholey, 2002]. Thus, SE stents are ideally suited for superficial locations such as the carotid and femoral arteries. Moreover radial strength need not be considered for SE stents, thus removing a central and limiting design constraint. This allows stent designers to focus on other issues such as smaller cell size and improved flexibility.

Radial stiffness is defined as much how the diameter of a stent is reduced by the application of external pressure. A BE stent will be much stiffer than SE stent of identical design because of the lower elastic modulus of Nitinol. The difference is hard to quantify sue to the non-linear stress-strain curve of Nitinol, but generally BE stents are three times stiffer [Duerig and Wholey, 2002]. Thus, BE stents are designed to have high radial strength and stiffer in nature than SE stents. Since the radial compliance of a SE stent is much greater than that of a BE stent, one can assume that a BE stent will in turn reduce the radial compliance of the blood vessel.

Axial stiffness which is reflected in the bending compliance is also much higher in SE stents. This has important ramifications in delivery and deployment, making SE stents more conformable, i.e., they adapt to the vessel geometry rather than force the vessel to the shape of the stent. It is plausible that forcing the vessel into an unnatural shape can lead to high contact forces at the end of the stents [Duerig and Wholey, 2002]. There are additional complications in stenting dynamic vessels such as the femoral, carotid, and subclavian vessels that BE stents cannot handle.

Acute recoil refers to the reduction in diameter that is immediately observed upon deflation of the balloon. A BE stent tends to recoil after the balloon is deflated, whereas SE stents aid the balloon inflation with no acute recoil. Although both types of stents recoil within the body due to the springback forces of the vessel, BE stents recoil less when placed in calcified regions [Duerig and Wholey, 2002]. Although SE stents can be made stiff like commercially available BE stents, many of the advantageous properties would be lost in such a design.

1.3.2. FEM Modeling of Stent Geometries

In this research, different FEM approaches will be investigated for Nitinol stents and compared to experimental results. The major goal of this research is to create an efficient FEM

method that can be used to accurately predict the behavior of different Nitinol stent geometries without the need for experiments. Only recently, numerical analyses (FEM) have been proposed as an alternative approach to investigate the mechanical properties of intravascular stents [Migliavacca et al., 2002]. Although FEM methodologies are well explored and used in many engineering fields, it is worth noting that the reliability of the results depends on the assumptions and hypotheses adopted in the analysis. Since the stent expansion models include geometric and material non-linearities, such simulations are often quite challenging.

Apart from the *in vitro* fluid dynamics studies on intravascular stents [Peacock et al., 1995] structural FEM analyses were used by Dumoulin and Cochelin [2000] to evaluate and characterize some properties of BE stents. Etave et al., [2001] used FEM analyses to compare the performance of two different types of stents, and Auricchio et al. [2001] who realized a 3-dimensional study of the stent artery interaction during stent deployment. Furthermore, Rogers et al. [1999] studied a 2-dimensional balloon artery interaction and Oh et al. [1994] utilized FEM to analyze the stress state of atherosclerotic arteries during balloon angioplasty. Moreover, Whitcher [1997] provided examples of the advantages in the use of FEM model in predicting the mechanical behavior of stents and balloons. Miglivacca et al. [2002] elucidated how the FEM models can be used in the optimization of the design of coronary intravascular stents with particular attention paid to the effects of different geometrical features on the mechanical performance of a commercially available stent.

The focus of this study is on the development of an appropriate material model for Nitinol, which as of yet has not been successfully done in the study of stent architecture. Furthermore, these material considerations are applied to four different stent geometries, which include the Guidant Absolute Stent, and IntraCoil Coil stent. The efficacy of the model is validated with comparison to experimental results for the two commercially available stents. The model is then used as a predictive study to measure the response of two proposed Nitinol SE stent designs. Thus, although much work has been done with regards to the modeling and validation of BE stents and stent-artery interaction, significant work needs to be done to build an accurate model that will eventually lead to the successful development and testing of stents *prior* to manufacture rather than the trial and error method commonly utilized in the industry today.

1.4 Research Issues and Thesis Organization

The ultimate goal of this research is an efficient method for analysis of the forced response of stents with respect to their geometry and material. The major research issues anticipated in realization of this goal are: (1) existing and new stent designs must be accurately and efficiently modeled by computer aided design (CAD) and imported to the FEM software; (2) comprehensive material model for Nitinol must be formulated and approximated in the FEM analysis; (3) the forced response and deformation of the stent must be measured by adequate experimental methods. This could be difficult because of the unusual geometry, material properties, and deformation that the stent undergoes; and (4) the theoretical forced response of stent must be validated by the experimental results for determination of the efficacy of CAD and FEM methodology and accuracy of their predictions.

The first step was to render the Absolute Stent Geometry using the CAD software Solidworks. Several different lengths of the stent geometry were create in anticipation of the increased computation time for longer stents. In particular three stents of length 7.30 mm, 10.87 mm, and 14.42 mm were tested using the FEM software COMSOL. The COMSOL modeling of the response of the Absolute stent to tensile loadings was considered. In order to determine whether COMSOL actually yields solutions reflective of real world physics, steel stents were first tested. It is hypothesized that the steel stents will exhibit less extension for the same applied loads. Once the tests for the Steel AISI 4340 work-material was complete, two different Nitinol material models were implemented and compared to each other as well as to the experimental results for the tensile tests. The simple linear elastic model for Nitinol was compared to a Nitinol model with plasticity constraints derived from the Helmholtz thermodynamic potential.

Comparison of the theoretical and experimental results was followed by the design and simulation of three proposed stent designs. These designs were included to show the change in stent deformation when subject to tensile loads. The three designs increased the bridge number, length, and changed the bridge position as test parameters. These were then compared to the actual Absolute stent geometry simulations.

1.4.1. CAD and FE Model Formulation of Commercial SE Stents

CAD model of the Guidant Absolute Stent is necessary for FEM analysis. In this research the Solidworks software was used to model the complex stent geometries. The technical

challenge is in balancing the accuracy of the geometry with the computational effort in CAD and FEM. Stent dimensions were recorded and implemented in the CAD model to ensure close correlation of physical structure. Two different CAD representations of the Absolute stent geometry were tested using the FEM software, COMSOL. A solid model and a beam model representative of the actual stent were imported into COMSOL for the finite element analysis.

In addition to the constitutive representations of the stents, a material model was also necessary, given the more complex nature of loading response of shape memory alloys (SMAs). Unlike steel alloys that exhibit a relatively linear relationship between stress and strain, superelastic metal alloys, like Nitinol exhibit a characteristic hysteresis for the same relation. This path dependent relationship between stress and strain makes the material model rather challenging. One cannot assume a constant modulus of elasticity as for steel alloys, but one that is defined by partial differential equations (PDEs) based on the phase of transformation. Given that Nitinol exhibits a solid phase change from martensite to austenite during the pre-loading and deployment stages of implantation during a coronary intervention procedure, care must be taken to ensure that the thermoelastic components of the material's behavior are accurately modeled. Thus, rather than use the prescribed PDEs for superelastic materials provided by the FEM software, it is necessary to manipulate these to accurately model the response of Nitinol to the various theoretical loadings. The material model and FEM loading used to validate the model for the Absolute and IntraCoil stents was used to test the loading response of two proposed stents specifically designed for stenting the femoropopliteal segment of the human body. Given the need to use a material with an elastic modulus that can handle the different mechanical stresses placed on it and retain its shape, a material model for Nitinol needed to be used. Since the stress-strain relationship for Nitinol has a pronounced hysteresis, or path dependence, it was not a trivial task to accurately model the response of the material to various loadings. The superelasticity of the material was difficult to model and added to the computational cost in determining the forced response of the various stent geometries. A biocompatible steel alloy was also modeled to compare the loading responses for two different materials. In addition two commercial stents and two novel proposed designs were tested.

COMSOL can successfully model the loading response, be it tensile, crush, or torsional, of SMAs. Nitinol is the SMA of concern here as it is a more suitable material for implantation in the femoral-popliteal region of the human body. As discussed earlier this region of the body

tends to experience unique mechanical stresses that conventional stainless steel stents cannot withstand over a long duration. As such, these stents are subject to various types of failures. Since Nitinol exhibits many of the elastic properties that natural materials do it is a suitable replacement. Unfortunately to produce and experimentally test Nitinol stents can be quite costly and demanding; thus, an effective material model would aid in the simulation of such stents under various loadings experienced within the body. As the experimental tensile loading of the stents was done at room temperature, the material model implemented in the FEM is also maintained at room temperature.

Using the CAD representation of the actual stent and FEM methodologies the response of the stent to various loading conditions was studied. In addition to the loading considerations, temperature effects were also explored. Since Nitinol exhibits responses to thermo-mechanical loadings an effective model needs to take the thermal effects into account. Although these were not simulated they provide an accurate gage of the usefulness of particular geometries in stenting the femoropopliteal segment of the human body.

1.4.2. Comparison of Experimental and Theoretical Results

The experimental loading results of the absolute stent were compared to the theoretical FEM models. The model physics were simulated as accurately as possible to align as closely with the experimental results. Once sufficient parity between experimental and theoretical results was obtained, the model was considered to be an accurate representation of real life conditions at room temperature. As such it could be used to test the loading response of other suggested geometries with confidence, thus, avoiding the resource intensive experimental methodologies currently used to manufacture and test stents.

1.4.3. FEM as a Tool for Prediction of Structural Integrity

FEM can be used as a tool to determine the response of the stent structure to various forced loading scenarios. The elongation of the stent can be related to the load that causes the stretch to form a relationship between the strain and the load. Moreover, the stress concentration along with the load-strain relationship can be used to determine loads at which the stent would see structural failure. Furthermore, these relationships can be used to identify the location of breaks and adjust the stent geometry pre-manufacture to prevent structural failure. FEM can be

used to determine the response of the stent to different loads, and thus, classify whether the stent is suitable for entrance into the manufacture phase of stent design.

1.4.4. Thesis Organization

In Chapter 2 the CAD models for two commercially available stents and two novel stent geometries are presented. The stent geometries are described in detail as is the methodology used to construct them in the Solidworks software. Moreover, the FEM modeling of the forced loading response is described. COMSOL was used to construct the material models for the Nitinol and steel alloy. The equations for the material model are discussed as is the FEM procedure as related to the COMSOL software. In addition the results from the theoretical forced response for the different stent geometries for the two different materials are presented. The experimental results of the stents are addressed in Chapter 3. Two commercial stents were subjected to tension loadings and the response measured and plotted for comparison to the FEM results. A comparison of the experimental and theoretical results is presented in Chapter 4. Any significant similarities and differences between the two are addressed here to determine the efficacy of the modeling procedures. Finally, conclusions and any future studies to improve the modeling and experimental methodologies are discussed in Chapter 5.

CHAPTER 2: FINITE ELEMENT MODELING OF STENT BEHAVIOR

2.1. Introduction

Modeling is a necessary tool to understand the material flow, stresses, and strains, which are difficult to measure experimentally. Modeling of stent behavior has been explored with regards to BE stents. However, the current modeling efforts are lacking in the application of FEM to SMA as they are used as a material for stent geometries. Although the literature is rich in numerical models able to describe the thermo-mechanical response of Nitinol, successful finite element analyses of SMA devices with commercial code is quite limited. Much of the literature focuses on the inflation, implantation, and stent-artery interaction of BE stents, generally constructed from stainless steel 316 or 316L. As such, the literature is limited in the FEM studies as related to Nitinol stents. This research effort becomes the goal of this study.

The Nitinol work-material has two important thermo-mechanical behaviors: (1) shape memory effect, and (2) pseudoelastic effect, which makes it useful in biomedical applications with qualities of resistance to corrosion, biocompatibility, fatigue resistance, MR compatibility, and kink resistance [Petrini et al., 2005]. These two behaviors allow the Nitinol to undergo large mechanical deformations and recover their original shape upon thermal loading, or simply by mechanical unloading. Of particular importance in this study is the pseudoelasticity of the work-material, i.e., the ability to recover the original shape after large deformations induced by the mechanical load. This allows it to maintain a constant force over a wide range of deformation [Petrini et al., 2005]. The material properties of SMAs can be explained by crystallography and thermodynamics. As discussed in chapter 1, the Nitinol is characterized by two solid phases: (1) Austenite, and (2) Martensite. The austenite phase is stable at temperatures above the austenite formation temperature, A_f, which is below room temperature, T_{room}. This phase exhibits high symmetry, as compared to the martensite phase, which is stable at martensite finish transformation temperature, M_f. The martensite can exist in two phases, the twinned multi-variant, or the de-twinned single variant, with differences arising due to the tendency of the SMA to minimize misfit with the surroundings in the twinned Martensitic phase [Petrini et al., 2005]. In the de-twinned phase the material has a tendency to align variants along a predominant direction, and, thus, be associated with macroscopic phase change.

When the Nitinol work-material is mechanically deformed at a temperature above A_f the stress induced transformation causes a phase change from the austenite to the single variant (de-twinned) martensite. Since the martensite is unstable at $T > A_f$, as soon as the load is removed, the reverse transformation takes place, and the material assumes its original shape. This pseudoelastic behavior is paramount to the functionality of the stent structure. During the loading and unloading the material response shows a hysteresis, i.e., when the direct and reverse transformations take place, the stress remains constant over a wide range of deformation. At temperatures below M_f, a stress induced change results in a transformation from the twinned martensite to de-twinned martensite phase. When the stress is removed, a residual deformation takes place, and heating the material to temperature above A_f at zero stress allows the material to recover the residual strain, and since the de-twinned phase is no longer stable at this temperature, a reverse change to the austenite phase occurs. However, reducing the temperature below M_f allows the material to return to the twinned martensite phase, with no apparent macroscopic deformation [Petrini et al., 2005]. This is termed shape memory effect. Since the Absolute Guidant Stent is present in the Austenite phase at $T_{room} > A_f$, this study focuses on pseudoelasticity as the mechanism of original shape recovery in all modeling applications.

The constitutive modeling of SMA and implementation into finite element codes is becoming an important tool for designers and a requirement for the Food and Drug Administration (FDA). In this study the commercial COMSOL® finite element code was developed to simulate the pseudoelastic mechanical response of the stent. The 3D model was chosen because the 2D axisymmetric model was unable to simulate the complicated stent geometry. Modeling results will show significant deformation due to tension, compression, crush, and torsional loads. In this study, FEM techniques were developed to test the *in vitro* forced loading response of the Absolute Stent, which were, in turn, validated via experimental measurements. Such a validation of the finite element analysis was done in order to demonstrate the efficacy of this technique in the design and development of novel stent geometries.

The next section reviews the existing literature as it relates, first to the finite element study of Nitinol SE stents, and second to the finite element simulation of stent geometries in general, irrespective of material considerations. Both are important to create the framework for this investigation, and to demonstrate the need for such studies as a means of resource and time conservation as related to the design and manufacture of stent geometries. Next the 3D CAD

formulation of the Absolute stent geometry is presented, followed by the modeling theory. In particular the material model for Nitinol and the mechanical model are thoroughly studied. Then, the finite element simulation of the stent model is presented, followed by the FEM analysis outputs. Lastly, relevant conclusions as related to the FEM of the Absolute stent are discussed.

2.2. Review of stent modeling

Computational analyses could provide access to an extensive amount of information under highly controlled conditions, and would make it more possible to screen different and competing stent design alternatives prior to costly prototype fabrication. In this context, an in-depth review of stent modeling is presented in this section. This literature review delves into the pertinent aspects of modeling for Nitinol stents in detail, followed by a more general discussion of the finite element modeling of BE stents. It is important to note that although the literature is rich in the FEM study of stent geometries, more attention has been given to BE stents.

Of particular importance are investigations that use finite element modeling in COMSOL to study the forced loading response of Nitinol stents. Ghosh et al., [2011] presented a numerical study on the mechanical properties of stents with different materials during stent deployment with balloon expansion. Although they consider Nitinol stents, it is important to note that mode of expansion simulated does not take advantage of the pseudoelastic effect. As such, this study may be considered ancillary. However, the authors define the work-material by specifying parameters such as Young modulus, Poisson ratio, density, etc. Although this can adequately simulate material behavior, this investigation goes beyond this simple definition of material parameters and models the material using the partial differential equation (PDE) module that the COMSOL software affords. Shrivastava [2006] modeled a beam fixed at either end using a thermodynamic constitutive model for Nitinol. Although the modeling of the stent structure was not attempted, it is worth noting the constitutive material model that Shrivastava used as a basis for building the material model used in this study. An analytical material model was developed by Thiebaud et al., [2006] and then implemented into COMSOL. This was used as the material model for the Nitinol work material in this investigation. Modeling material behavior needs a thermodynamic potential and also a dissipation potential or some yield functions of phase transformation. Thus, a Helmholtz free energy and two yield functions are used to define the

forward and reverse transformations from the austenite to martensite and back. This thermo-mechanic model for the pseudoelasticity is further developed in Section 2.

Petrini et al., [2005] developed a three-dimensional constitutive model within the framework of phenomenological continuum thermodynamics. The authors assumed the strain and the absolute temperature as the control variables, and a traceless second order transformation tensor as the internal variable. Thus, the model was able to distinguish between a generic parent and product phase. It is important to note that the authors assumed a small strain regime, which was justified since in the application of stents large displacements are generated but small strains are induced. A similar small deformation theory is used in this investigation. The authors derived the constitutive equations from standard arguments, which is developed in Section 2.4.1, and applied it to a coronary stent. The stent was chosen because it is one of the most diffused applications of the pseudoelastic Nitinol in the medical field, and because of its availability for the comparison of numerical and experimental results. The Nitinol stent, in the austenitic phase, at room temperature ($T_{room} > A_f$), was mounted onto a catheter and compressed by a protective sheath. Once the catheter reached the site of the blockage, the sheath was retracted, and the stent expanded into the artery taking advantage of the pseudoelastic effect.

Petrini et al., [2005] verified the model's ability to describe SMA devices that exploit pseudoelasticity by comparison with experimental results of a crush test, which consisted of compressing the stent between two planes parallel to the stent longitudinal axis. They developed a 3D CAD model of the coronary stent and performed a numerical analysis, similar to this investigation. The displacement control was assumed and a dynamic simulation with an implicit formulation was used to provide integration of the stress/displacement response of the device. This approach, assured a major stability of the solution and of the strongly non-linear problem. Since it was impossible to perform experimental tests on the sole stent material as it was unavailable, the authors mentioned that the continuum mechanical model cannot be used as a validation of the material constitutive model. It is important to note that agreement between the numerical and experimental curves is an encouraging result that shows numerical results can give insight into stress and strain distribution, thus, providing opportunities for design optimization. The authors noted that proper changes in some stent features could produce a design where strain is well distributed throughout the stent, and hence a large percentage of the material exploits pseudoelasticity with very low risk of overcoming maximum recoverable strain

limit and with high deformation recovery. A similar approach is adopted in this investigation with the agreement of experimental numerical results used as a platform for testing variations in stent geometry.

Migliavacca et al., [2004] developed a material model for the shape memory alloy coronary stents and their interactions with the vascular wall. As in the Petrini study, they modeled the pseudoelastic effects of the Nitinol work-material. However, rather than develop a material model based on constitutive equations, they simply used the following material properties: Young modulus, E, assumed equal for the austenite and martensite; stress value, σ_o, indicating the mean value of the mechanical hysteresis; maximum transformation strain, ϵ_L, reached at the end of the austenite to martensite transformation; measure of the mechanical hysteresis amplitude, R; and the stress threshold value, σ_s, at which the austenite to martensite transformation starts. They found that a small percentage of the material exploited the pseudoelasticity with higher risk of overcoming maximum recoverable strain limit. They concluded that the results of the FEM analysis show how the computational methodology can be easily applied to the new generation of coronary stents and can be useful to develop comparative between different types of devices. As such, the motivation of this study becomes further developed given the applicability demonstrated by Migliavacca et al.

Conti [2007] presented an engineering model of Nitinol, and conducted numerical simulations as part of a Master's Thesis. The creation of a robust material model to numerically implement the superelastic behavior of Nitinol requires one to understand the thermodynamic process involved and the macroscopic effects. The model developed based on the microscopic behavior of a single crystal has been shown to agree with experimental results, but is not practical from an engineering standpoint. An engineering constitutive equation must include: influence of the initial conditions (T, σ) on phase transformation, different stress thresholds for each phase transformation to perform the hysteresis, and the reversibility of the phase transformation by thermo-mechanical cycles. Conti noted that most of the mechanical testing data that is available is uniaxial since Nitinol is typically available as relatively thin wires and tubes. It is important to note that the uniaxial behavior is easy to reproduce compared to the model that represents the m-D stress strain behavior. Conti noted that the numerical implementation of the Nitinol superelasticity is beyond the scope of his work (as it is here) and goes on to present the material routine used in the commercial ABAQUS code. As with Petrini

et al., a small strain regime is assumed, and the total strain (ϵ) was decomposed into two parts: a purely linear elastic component (ϵ^{el}) and a transformation component (ϵ^{tr}), which was also assumed to be the internal variable. The model was a Mechanism Based Continuum Mechanics Model based on generalized plasticity.

In addition to the studies of the mechanics of Nitinol SE stents, several studies have been conducted to study the expansion and interaction with the arterial wall of balloon expandable stents. These include, but are not limited to, a numerical investigation of the intravascular coronary stent flexibility [Petrini et al., 2004], a predictive study of the mechanical behavior of coronary stents by computer modeling [Migliavacca et al., 2005], mechanical behavior of coronary stents investigated through the finite element method [Miglivacca et al., 2002], finite element analysis of the implantation of a balloon-expandable stent in a stenosed artery [Liang et al., 2005], practicability and limitations of finite element simulation of the dilation behavior of coronary stents [Stolpmann et al., 2003], finite element simulation of stent expansion [Chua et al., 2002], analysis of the transient expansion behavior and design optimization of coronary stents by finite element method [Wang et al., 2006], cardiovascular stent design and vessel stresses by finite element analysis [Lally et al., 2005], analysis of the mechanical performance of a cardiovascular stent design based on micromechanical modeling [McGarry et al., 2004], mechanical response of a metallic aortic stent based on a beam-on-elastic foundation model [Wang and Chandar, 2004], cardicoil stent-artery interaction [Brand et al., 2005], and effects of stent structure on stent flexibility measurements [Mori and Saito, 2005].

Based on the literature review the current modeling efforts are lacking in the application of FEM to SMA as they are used as a material for stent geometries. Although the literature is rich in numerical models able to describe the thermo-mechanical response of Nitinol, successful finite element analyses of SMA devices with commercial code is quite limited. Much of the literature focuses on the inflation, implantation, and stent-artery interaction of BE stents, generally constructed from stainless steel 316 or 316L. The mechanical behavior of the Guidant Absolute stent is not well explored, and neither is the effect of stent geometry on mechanical behavior. Although several material models for Nitinol exist it is important to note that the material model has not been applied to study such stent geometry. This study aims to create a more comprehensive numerical simulation of Nitinol stent that can be used in the treatment of atherosclerotic lesions in the popliteal segment of the femoral artery. Furthermore, comparisons

to experimental results are not always present in the literature, and attention has been paid to the validation of the numerical results with different experimental techniques. Although most studies use material parameters to define the Nitinol material, this study uses both the PDE formulation of the material model, as well as the simpler method of parameter specification, as allowed by the commercial COMSOL FEM software. Thus, an inclusive numerical model that encompasses all forms of loading is carried out in this investigation and validated with experimental methodologies that load the stent specimen in conjunction with the aforementioned numerical simulations.

2.3. CAD model of stent geometry

The software Solidworks® was used to do the CAD rendering of the Guidant Absolute stent geometry. A hollowed cylinder was first extruded in the drawing environment. The inner and outer radii of the cylinder were specified in accordance with the measurements taken of the Guidant Absolute stent. The inner diameter was measured to be 5.36 mm and the outer diameter was 5.46 mm. The thickness of the extruded cylinder was 0.10 mm; this was as close to the measured thickness of the stent using an electrical caliper. Next a rectangle with width π*D = 17.15 mm was drawn in a plane parallel through the cylinder's axis of rotation. This rectangle was used to measure the spacing of the individual struts and bridges (Figure 2.1(a)).

Since the Absolute stent has 6 bridge points per strut, the space between each bridge point to the next strut was determined to be 2.858 mm. In addition to the horizontal spacing of each strut, with a standard caliper the length of the bridges was determined to be 1.778 mm. Once the first strut row had been laid out, the "linear pattern" tool in Solidworks was used to repeat the entire 17.15 mm row, the length of the drawn stent, which was easily altered by changing the length of the extruded hollow cylinder. Once the linear pattern had been extended the desired length, the bridges connecting the strut rows were drawn. It is important to note that the bridges alternated position on each individual strut row, and between alternating rows of struts, i.e., the position of the bridges were staggered such that the connection point between each strut row alternated down the length of the stent.

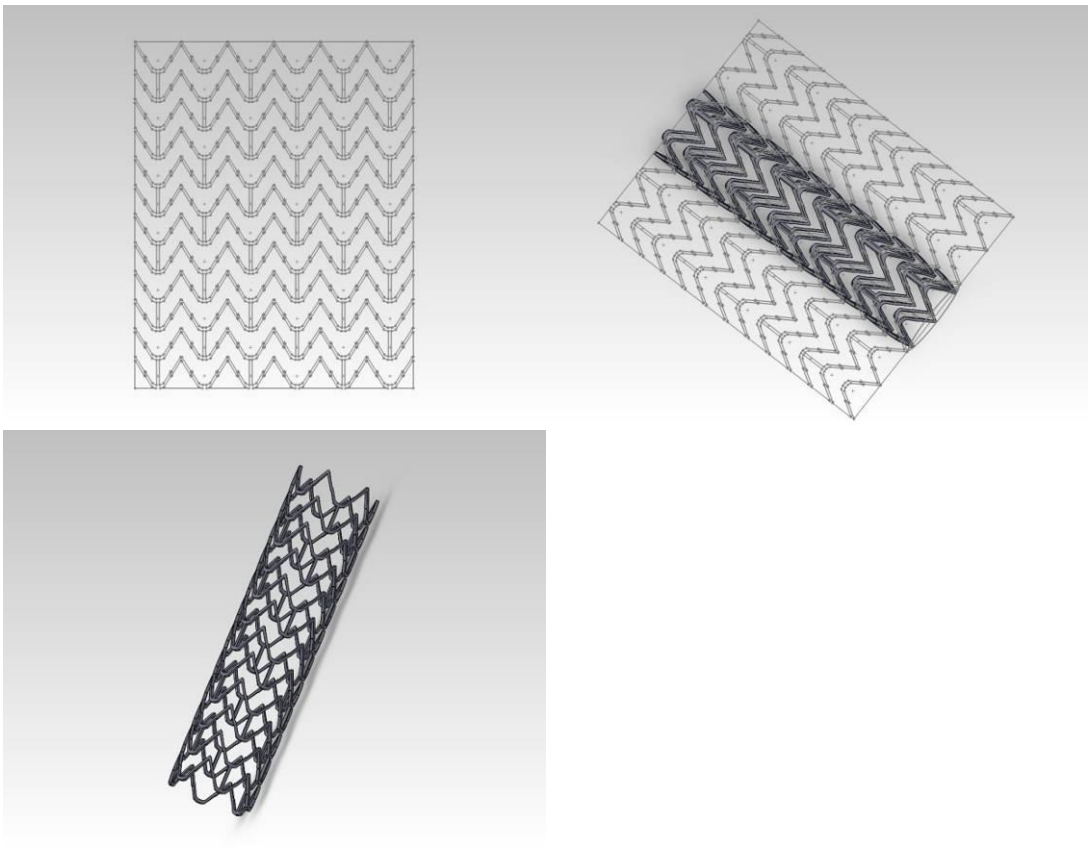

Figure 2.1 (a) (top left) Absolute Stent Pattern, (b) (top right) wrap function, (c) completed stent

One challenging aspect of the CAD formulation of the Absolute stent geometry was the use of the "wrap" tool in Solidworks. For successful CAD modeling the entire pattern to be embedded into the 0.10 mm thick hollow cylinder had to be a closed loop with no intersecting elements (Figure 2.1(b)). Given that there were several rows of the pattern, the task of ensuring that no open or intersecting elements were present was challenging. If the pattern had any errors, the implementation of the "wrap" tool failed, and the pattern had to be reviewed and corrected. For example, if the need was to generate two markers to designate screw position, two circles could be drawn on a plane tangent to the cylinder surface, and embedded into the surface using this tool, i.e., concentric or independent circles could be imbedded, but interesting circles, or arcs could not. In effect, the "wrap" tool took the rectangular pattern, rotated it around the face of the hollow cylinder, and removed any material that was not part of the closed loop, rendering a 3-D representation of the stent of interest (Figure 2.1 (c)).

Stents of 7.30, 10.87, 14.42, 21.54, 42.90, and 67.82 mm were drawn. Figure 2.2 (a-c) shows the 7.30, 10.87, and 14.42 mm Absolute stents, which were theoretically tested for various

uniaxial loading conditions. It is important to note that the stent could not be cut axially to use the symmetry condition, because of the staggered position of the bridges between the struts. Although there is rotational symmetry this cannot be used to apply symmetry boundary conditions. As such, entire cylindrical stents of the three aforementioned lengths were tested. Moreover, stents of different lengths were rendered by CAD in anticipation of the increased computation time necessary to calculate the reaction forces due to uniaxial forced loadings for each stent. As such an envelope of simulation parameters could be formed and explored.

(a)  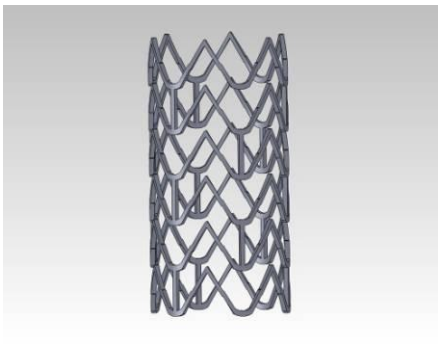 (b)

(c) 

Figure 2.2: Stent Lengths Tested, (a) 7.30, (b) 10.87, (c) 14.42 mm

2.4. FEM theory

This section presents the mathematical formulations of material and mechanical modeling, including continuum mechanics as related to the deformation of the stent structure. Equations describing the Nitinol work-material under tension and compression were formulated assuming a continuous media. The three basic components discussed here are kinematics, conservation laws, and constitutive equations in the presence of an internal state variable. The kinematics component describes the geometry of motion and deformation of the stent structure irrespective of the cause of the deformation. The conservation laws show how external effects influence the deformation, and finally, the constitutive equations allow for a mathematical description of the

characteristic material behavior. The geometry of deformation of the stent structure and effect of external factors, e.g., tension, compression are determined internally by COMSOL software. However, the mathematical description of the material characteristics was modeled with a PDE describing the thermodynamic potential in the presence of an internal state variable. Before proceeding the material modeling and mechanical response in detail, a brief review of continuum mechanics is presented here in adherence with the thermo-mechanical constitutive modeling presented by Lagoudas [2008].

Kinematics allows us to relate the position of the Nitinol material point in a deformed configuration to the same material point in the reference configuration by the displacement vector field **u**(**X**, t), where **X** is the reference position of the material point. From here a measure of the deformation of the neighboring material points can be defined as the deformation gradient tensor, ***F***;

$$\boldsymbol{F = \nabla u + 1} \tag{1}$$

Where $\boldsymbol{\nabla u}$ is the displacement gradient and **1** is a second order identity tensor. From here the symmetric second order *Green-Lagrange* strain tensor, *E*, can be defined as;

$$\boldsymbol{E = \frac{1}{2}\left[F^T F - 1\right]} \tag{2}$$

The expression for the *Green-Lagrange* tensor can be rewritten with respect to $\boldsymbol{\nabla u}$ as;

$$\boldsymbol{E = \frac{1}{2}[(\nabla u) + (\nabla u)^T + ((\nabla u^T)(\nabla u))]}. \tag{3}$$

It is important to note that the idea of choosing a reference configuration is more complicated for a SMA, like Nitinol, due to the existence of two natural reference configurations, i.e., stress free configuration in the austenitic and Martensitic phases, as compared to other more conventional materials like steel. The Guidant Absolute stent exists in stress free austenitic configuration at $T_{room} > T_{Af}$, and this is chosen as the reference configuration, with the transition of austenite to martensite introduced as the internal state variable, introduced in the subsequent sections.

The framework for the modeling of Nitinol can be simplified if one assumes that the deformation gradient tensor, ***F***, approaches the identity tensor, **1**, or for small displacement gradients, the quadratic term in (3) can be neglected, and the difference between the reference and deformed configuration becomes negligible. This small deformation assumption is valid because the strains generated are small compared to the deformation, and the infinitesimal strain tensor, □, can be defined as;

$$\varepsilon = \frac{\mathbf{1}}{\mathbf{2[(\nabla u) + ([\nabla u])^T]}} \quad (4)$$

The displacement gradient in the infinitesimal strain tensor can be defined over the deformed configuration of the stent because the difference between the two configurations is a higher order effect [Lagoudas, 2008]. This strain tensor is used in the further development of the FEM model.

In addition to the kinematics of Nitinol work material, conservation of mass, linear momentum, angular momentum, and energy are used to develop the model. In continuum thermodynamics, the conservation of energy is the first law of thermodynamics, and the second law relates to the principle of entropy. A review of these laws is presented as a precursor to the development of the material model, and mechanical response of the stent specimen. Conservation of mass states that the total mass of a continuum body cannot change with time or deformation. If one considers the mass of the stent specimen, *M*, as related to the density, □, $M = \int_{\Omega} \rho dV$, where *V* is the volume of the sample. The law of conservation of mass can be written as;

$$\frac{DM}{Dt} = \frac{D}{Dt}\left(\int_{\Omega} \rho dV\right) = \mathbf{0} \tag{5}$$

where $\frac{D}{Dt}$ is the material time derivative and following standard derivations in continuum mechanics the local form of the conservation of mass can be determined to be;

$$\frac{\delta \rho}{\delta t} + div(\rho \boldsymbol{v}) = \mathbf{0} \tag{6}$$

where $\boldsymbol{v}$ is the velocity of the material point, and the divergence operator acts on the vector field in the deformed configuration.

Conservation of linear momentum states that the rate of change of linear momentum in a continuum body is equal total sum of surface and body forces applied to it. The integral form of the conservation of linear momentum is given by;

$$\frac{D}{Dt}\left(\int_{\Omega} \rho \boldsymbol{v} dV\right) = \int_{\delta\Omega} \boldsymbol{t} dS + \int_{\Omega} \boldsymbol{b} dV \tag{7}$$

where $\boldsymbol{t}$ is the surface traction, S is the entropy, and $\boldsymbol{b}$ is the body force vector. The local form of the conservation of linear momentum can be derived as;

$$div\,(\boldsymbol{\sigma}) + \boldsymbol{b} = \rho \dot{\boldsymbol{v}} \tag{8}$$

Where $\boldsymbol{\sigma}$ is the Cauchy stress tensor, and the divergence operator acts on the stress tensor. The acceleration of a specific material point is given by $\dot{\boldsymbol{v}}$. Since this study focuses only on linear deformation of the stent the conservation of angular momentum, which states that the rate of

change of angular momentum is equal to the sum of the momentum applied by the surface and body forces, is not discussed here. Conservation of energy, or the first law of thermodynamics states that the time rate of change of the total energy of the stent is equal to the rate at which mechanical work is done on the stent by surface traction and body forces, plus the rate at which thermal energy is added by heat flux, $\boldsymbol{q}$, and other heat sources, $\boldsymbol{r}$. The integral form of the conservation of energy is given by;

$$\frac{D}{Dt}\left(\int_{\Omega}\frac{1}{2}\rho \boldsymbol{v}.\boldsymbol{v}dV+\int_{\Omega}\rho u dV\right)=\int_{\delta\Omega}\boldsymbol{t}.\boldsymbol{v}dS+\int_{\Omega}\boldsymbol{b}.\boldsymbol{v}dV+\int_{\delta\Omega}-\boldsymbol{q}.\boldsymbol{n}dS+\int_{\Omega}\rho r dV \tag{9}$$

Since the experimental parameters indicate that there was no heat exchange between the stent and the environment, the last two terms from Eq. (9) can be dropped and the rate of change of energy can be related to the surface traction and body forces only as;

$$\frac{D}{Dt}\left(\int_{\Omega}\frac{1}{2}\rho \boldsymbol{v}.\boldsymbol{v}dV+\int_{\Omega}\rho u dV\right)=\int_{\delta\Omega}\boldsymbol{t}.\boldsymbol{v}dS+\int_{\Omega}\boldsymbol{b}.\boldsymbol{v}dV \tag{10}$$

where $\boldsymbol{u}$ is the specific internal energy. The local form of (10) can then be written as $\boldsymbol{\rho}\dot{u}=\boldsymbol{\sigma}:\dot{\varepsilon}$. The (:) indicates a double dot product between the two tensors, and $\dot{u}$ and $\dot{\varepsilon}$ indicate the material time derivatives of the specific internal energy and infinitesimal strain tensor respectively [Lagoudas, 2008].

The second law of thermodynamics states that the internal entropy generation is always greater than or equal to 0. Mathematically this can be expressed as the Clausius-Duhem inequality;

$$\frac{D}{Dt}\left(\int_{\Omega}\rho s dS\right)+\int_{\delta\Omega}\frac{\boldsymbol{q}}{T}.\boldsymbol{n}dS-\int_{\Omega}\frac{\rho r}{T}dV\geq\boldsymbol{0} \tag{11}$$

Since we are assuming an adiabatic interaction between the stent (body) and the environment the contribution of $\boldsymbol{q}$ and $\boldsymbol{r}$ is negligible, and the Clausius-Duhem inequality reduces to;

$$\frac{D}{Dt}\left(\int_{\Omega}\rho s dS\right) \geq 0 \tag{12}$$

and the local form of the inequality is given by $\rho \dot{s} \geq 0$.

Taking a look at the number of unknown fields and available equations reveals that there are a total of 18 unknowns and only 11 equations. Starting with the stress and strain tensors, there are six components from $\boldsymbol{\sigma}$, and six from $\boldsymbol{\varepsilon}$. In addition there are three unknowns from $\boldsymbol{u}$, and three additional unknowns from the temperature, density, and internal energy, all of which are scalar functions. In turn, there is one equation from conservation of mass, three from the conservation of linear momentum, one from the conservation of energy, and six equations from kinematics. There is a need for 7 more equations to construct a system with unique solutions, and these can be found by introducing the appropriate constitutive equations. This is presented in the following section, which is followed by a discussion of the COMSOL software mathematics and its internal calculation of elongation, shortening, and associated forces and stresses.

2.4.1. Material modeling

Constitutive equations are mathematical models intended to describe the principal features of the Nitinol work-material behavior in an idealized form [Lagoudas, 2008]. Since the Nitinol undergoes a stress induced phase change, it is characterized by a series of thermodynamic states that can be described by the introduction of additional internal state variables, like the Martensitic volume fraction. The equations used to describe the material behavior in the COMSOL environment are presented here, with attention paid to derivation of constitutive equations in the presence of internal state variables.

Thermodynamic state variables are those that represent all quantities that characterize the Nitinol in a certain state [Lagoudas, 2008]. If these variables are observable, they are external state variables; otherwise they are referred to as internal state variable. The thermodynamic state of the Nitinol work-material can be fully expresses by a combination of the external and internal

state variables. It is useful to review the concept of a thermodynamic potential, a function that characterizes a certain thermodynamic state of the Nitinol, and is dependent upon the state variables. Four thermodynamic potentials are generally chosen from: specific internal energy, $\boldsymbol{u}$, specific Helmholtz free energy, $\boldsymbol{\psi}$, specific enthalpy, $\boldsymbol{h}$, and specific Gibbs free energy, $\boldsymbol{G}$. $\boldsymbol{u}$ is a measure of the kinetic and potential energy of the material, while $\boldsymbol{\psi}$ is defined to be the portion of the internal energy available for doing work at a constant temperature [Lagoudas, 2008]. $\boldsymbol{h}$ is the portion of the internal energy that can be released as heat at a constant applied stress, and $\boldsymbol{G}$ is the portion of enthalpy available for doing work at a constant temperature.

Although the natural choice for the thermodynamic potential is $\boldsymbol{u}$, because it is a function of $\boldsymbol{S}$, a not easily measured quantity, one of the other thermodynamic potentials is more suited for the description of the Nitinol. Enthalpy is not commonly used for the same reason, which leaves $\boldsymbol{\psi}$ and $\boldsymbol{G}$. The choice between these two is contingent on which state variable is controlled during the experimental testing, i.e., stress (G) or strain (ψ). Since the elongation and contraction of the stent were measured, the strain was the controlled internal variable, and the Helmholtz free energy is selected as the thermodynamic potential. To determine the constitutive equations for Nitinol the independent and dependent state variables need to be identified.

The independent and dependent state variables characterize the behavior of the Nitinol work material. The following presents the relationship between the Helmholtz free energy and the specific internal energy obtained via a Legendre transformation:

$$\psi = u - sT \tag{13}$$

T, ε, and ζ represent the independent variables, where ζ represents a set of internal state variables. Since a simple material is one for which, the stress at each material point can be determined from a function of the local configuration history at the specified point, one can add the history of the temperature, temperature gradient, heat flux, internal energy, and entropy to the list of dependent variables. Thus, the constitutive behavior of a Nitinol work material point depends on ψ, $\boldsymbol{\sigma}$, s, and $\boldsymbol{q}$, which in turn depend on ε, T, $\boldsymbol{\nabla T}$, and ζ, which accounts for the loading path dependence of the shape memory alloy [Lagoudas, 2008]. The response functions are dependent on the $\boldsymbol{\nabla T}$, i.e., $\boldsymbol{g}$, and not on the gradient of ε and ζ. It is important to note that the response functions are

the simplification of the functions obtained when the Green-Lagrange strain tensor, $\boldsymbol{E}$, is decomposed to the infinitesimal strain tensor ε, $\boldsymbol{g}$, and ζ, and are assumed to be the same in both the reference and deformed configurations [Lagoudas, 2008]. Moreover, the response functions depend on the assumption of the principle of equipresence, which states that a quantity present as an independent variable in constitutive equation will be present in all, unless its presence contradicts physics or symmetry of the material.

With the response functions, the constitutive equations can be obtained with the realization that that every thermodynamic process of the body must obey the entropy inequality at all times, t, for each material point of the body. Moreover, for each material point an any given time, the variables ε, $\dot{\varepsilon}$, T, $\dot{T}$, $\boldsymbol{g}$, $\dot{\boldsymbol{g}}$, ζ, and $\dot{\zeta}$ can be varied independently and $\dot{T}, \dot{\boldsymbol{g}}, \dot{\zeta}$ are not arguments in the response functions. Now, substituting the reduced form of the first law of thermodynamics (12), and the time derivative of the Legendre transformation (13) into the Clausius-Planck inequality (15) the following form of the second law can be obtained:

$$\boldsymbol{\sigma}:\dot{\varepsilon} - \rho\dot{\psi} - \rho s\dot{T} \geq 0. \tag{14}$$

Next, it is possible to find the time derivative of the Helmholtz free energy, assuming that $\boldsymbol{\psi}$ is a continuous function. The chain rule of differentiation can be used to obtain the time derivative as:

$$\dot{\psi} = \frac{\delta\psi}{\delta\varepsilon}:\dot{\varepsilon} + \frac{\delta\psi}{\delta T}\dot{T} + \frac{\delta\psi}{\delta \boldsymbol{g}}\cdot\dot{\boldsymbol{g}} + \frac{\delta\psi}{\delta\zeta}\cdot\dot{\zeta}. \tag{15}$$

Substituting (15) into (14) yields the following equation:

$$\boldsymbol{\sigma}:\dot{\varepsilon} - \rho\left[\frac{\delta\psi}{\delta\varepsilon}:\dot{\varepsilon} + \frac{\delta\psi}{\delta T}\dot{T} + \frac{\delta\psi}{\delta \boldsymbol{g}}\cdot\dot{\boldsymbol{g}} + \frac{\delta\psi}{\delta\zeta}\cdot\dot{\zeta}\right] - \rho s\dot{T} \geq 0. \tag{16}$$

If all the variables ε, $\dot{\varepsilon}$, T, $\dot{T}$, **g**, ζ, and $\dot{\zeta}$ are fixed, but $\dot{\boldsymbol{g}}$ varied, it becomes evident that since $\dot{\boldsymbol{g}}$ can take on either positive or negative values, $\frac{\delta\psi}{\delta \boldsymbol{g}} \equiv \mathbf{0}$, and the Helmholtz free energy is not a function of the gradient of temperature, namely $\boldsymbol{g}$. Furthermore, due to the principle of equipresence, no other state variable depends on $\boldsymbol{g}$ either. If all the independent variables and their increments except for $\dot{T}$ are fixed, the entropy can be define to be:

$$s = -\frac{\delta\psi}{\delta T}. \tag{17}$$

Similarly the constitutive equation for the stress can be determined as:

$$\boldsymbol{\sigma} = \rho \frac{\delta\psi}{\delta\varepsilon} \tag{18}$$

And the Clausius-Planck relationship can be written as:

$$-\rho \frac{\delta\psi}{\delta\zeta} \cdot \dot{\zeta} \geq 0. \tag{19}$$

Depending on the specific form of the Helmholtz free energy the response function for the stress and entropy can be determined from (18) and (17) respectively. The response function associated with the heat flux, **q**, can be ignored since it was determined that the mechanical loading of the Guidant Absolute temperature is done adiabatically at room temperature. To complete the list of response functions, it becomes evident that $\dot{\zeta}$ must satisfy (19), and the necessary 7 equations are given by (17-19) to form a unique solution to the material behavior aspect of this modeling problem.

This general derivation of the constitutive equations for the Nitinol work material is done using the Helmholtz free energy, even though the Gibbs free energy is customarily used to define the thermo-mechanical loading path for SMAs in the stress-temperature space, because the temperature dependence of the Nitinol work material contributes to the shape memory effect mode of original configuration recovery. However, the Nitinol stent used in the experimental procedures employed only the pseudoelastic effect for recovery of its original configuration (shape). As such the derivation of constitutive equations, in the presence on internal state variables, needs to be applied to the specific instance of the Guidant Absolute stent to account for this mode of shape recovery.

Choosing a quadratic polynomial form of the Helmholtz free energy and specifying the natural independent variables to be $\boldsymbol{\varepsilon}$, and $\boldsymbol{T}$, with a traceless second order transformation strain tensor $\boldsymbol{e}^{tr}$ as the internal state variable, replacing ζ, in the general derivation (16), above, yields the following:

$$\psi(\boldsymbol{\varepsilon}, \boldsymbol{e}^{tr}, T) = \frac{1}{2}K\theta^2 + G\|\boldsymbol{e} - \boldsymbol{e}^{tr}\|^2 - 3\alpha K(T - T_o) + \beta\langle T - M_f\rangle\|\boldsymbol{e}^{tr}\| + \frac{1}{2}h\|\boldsymbol{e}^{tr}\|^2 + \tau_{\varepsilon_L}(\boldsymbol{e}^{tr}) \quad (20)$$

Where θ and $\boldsymbol{e}$ are the volumetric and deviatoric components of the total strain, $\boldsymbol{K}$ is the bulk modulus, G, $\boldsymbol{\alpha}$ the thermal expansion coefficient, $\boldsymbol{T}_o$ a reference temperature, $\boldsymbol{\beta}$ a material parameter related to the dependence of the stress inducing transformation on the temperature, and the $\langle\rangle$ the positive part of the argument, $\boldsymbol{h}$ a material parameter defining the slope of the linear stress transformation strain relation in the uniaxial case, and $\tau_{\varepsilon L}$ is an indicator function introduced to satisfy the constraint on the transformation strain norm [Petrini et al., 2005], where:

$$\tau_{\varepsilon_L}(\boldsymbol{e}^{tr}) = \begin{cases} 0 & if\ \|\boldsymbol{e}^{tr}\| \le \varepsilon_L \\ \infty & if\ \|\boldsymbol{e}^{tr}\| > \varepsilon_L \end{cases} \quad (21)$$

The constitutive equations describing the material behavior can be determined from standard arguments as follows. The volumetric component of the stress can be determined by differentiating $\boldsymbol{\psi}$ with respect to the volumetric component of the total strain as,

$$p = \frac{\delta \psi}{\delta \theta} = K[\theta - 3\alpha(T - T_o)]. \tag{22}$$

Similarly, the deviatoric component of the stress can be determined as the partial derivative of the Helmholtz free energy with respect to the deviatoric component of the stress as,

$$\boldsymbol{s} = \frac{\delta \psi}{\delta \boldsymbol{e}} = 2G(\boldsymbol{e} - \boldsymbol{e}^{tr}). \tag{23}$$

Furthermore, the equation for entropy can be found to be,

$$\eta = -\frac{\delta \psi}{\delta T} = 3\alpha K\theta - \beta \|\boldsymbol{e}^{tr}\| \frac{\langle T - M_f \rangle}{|T - M_f|} \tag{24}$$

The final constitutive equation relating the thermodynamic force associated with the transformation strain and indicated as transformation stress is found by differentiating $\boldsymbol{\psi}$ with respect to the internal variable,

$$\boldsymbol{X} = -\frac{\delta \psi}{\delta \boldsymbol{e}^{tr}} = \boldsymbol{s} - \boldsymbol{\alpha} \tag{25}$$

In (25) $\boldsymbol{\alpha}$ plays a role similar to that of yield stress in classical plasticity, and can be defined as,

$$\boldsymbol{\alpha} = [\beta\langle T - M_f\rangle + \boldsymbol{h}\|\boldsymbol{e}^{tr}\| + \gamma]\frac{\delta\|\boldsymbol{e}^{tr}\|}{\delta\boldsymbol{e}^{tr}}\ , \tag{26}$$

where $\beta\langle T - M_f\rangle$, and $\boldsymbol{h}\|\boldsymbol{e}^{tr}\|$ define the linear dependence of $\boldsymbol{\alpha}$, on the temperature and a linear hardening proportional to $\|\boldsymbol{e}^{tr}\|$ during the phase transformation. $\boldsymbol{\gamma}$ is defined as the sub-differential of the indicator function [Petrini et al., 2005], and is equal to zero if $\boldsymbol{e}^{tr}$ is greater than or equal to 0, and less than the transformation strain ε_L. Otherwise, $\boldsymbol{\gamma}$ is greater than or equal to 0, if $\boldsymbol{e}^{tr}$ is equal to the transformation strain. The material model is complete upon introduction of an associate law for $\boldsymbol{e}^{tr}$;

$$\dot{\boldsymbol{e}}^{tr} = \frac{\dot{\zeta}\left(\delta F(\boldsymbol{X})\right)}{\delta\boldsymbol{\sigma}} \tag{27}$$

Imposing the Kuhn-Tucker conditions, $\dot{\zeta} \geq 0, \quad F \leq 0, \dot{\zeta}F = 0$, where $\dot{\zeta}$ is similar to the plastic consistent parameter and $\boldsymbol{F}$ is a limit function. These parameters become more understandable when one considers a uniaxial tensile test, as was conducted in this study. In this case the yield function becomes, F(X) = |X|-R, and the stress deviatoric component is given by s = s_o+h|e^{tr}|+R. The term s_o = β<T-M_f> represents the initial mean value of the mechanical hysteresis, and varies linearly with temperature starting at T=M_f. Thus, the s_o+ R, which is the stress deviatoric component inducing transformation, also depends linearly on temperature. In particular for the transformation from austenite to single variant martensite at T=A_f, s^{as} = β(A_f-M_f)+R. Figure 2.3 shows the uniaxial stress strain curves for Nitinol at T=A_f (pseudoelasticity), and is used to define the material via the implementation of the presented equations in the COMSOL environment.

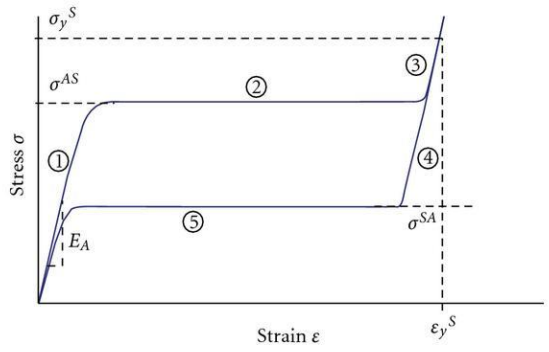

Figure 2.3: Pseudoelastic effect [Petrini, 2005]

Implementation of these constitutive equations in the presence of an internal state variable, describes the path dependent loading behavior of the Nitinol work material. Solving these in conjunction with the equations of structural mechanics will yield a visual solution describing the behavior of the Absolute stent subject to various tensile and compressive theoretical loadings.

2.4.2. Mechanical Response

The COMSOL code integrates the equations of motion explicitly through time. The term "explicit" means the state at the end of an increment is based solely on the displacements, velocities, and accelerations at the beginning of the increment. For 3D geometries, like the Absolute stent, solid, stress-strain application mode is used for stress analysis and general structural mechanics simulations. A brief overview of the theoretical structural mechanics is presented here followed by a review how the structural mechanics theory is implemented in the software.

The COMSOL structural mechanics branch is based on two relationships: strain-displacement, and stress-strain. It is possible to completely define the strain conditions at a point with the deformation components (u,v,w) in 3D, and their derivatives. The shear strain can be expressed in tensor form as ε_{xy}, ε_{xz}, ε_{yz}. The structural mechanics module assumes a small displacement regime, and the normal and shear strain components are given from the deformation as:

$$\varepsilon_x = \frac{\delta u}{\delta x}, \varepsilon_y = \frac{\delta u}{\delta y}, \varepsilon_z = \frac{\delta u}{\delta z}, \tag{28}$$

$$\varepsilon_{xy} = \frac{1}{2}\left(\frac{\delta u}{\delta y} + \frac{\delta u}{\delta x}\right), \varepsilon_{xz} = \frac{1}{2}\left(\frac{\delta u}{\delta z} + \frac{\delta u}{\delta x}\right), \varepsilon_{yz} = \frac{1}{2}\left(\frac{\delta u}{\delta z} + \frac{\delta u}{\delta y}\right) \tag{29}$$

The symmetric strain tensor, ε, consists of both the normal and shear components, and can be represented as,

$$\varepsilon = \begin{matrix} \varepsilon_x & \varepsilon_{xy} & \varepsilon_{xz} \\ \varepsilon_{xy} & \varepsilon_y & \varepsilon_{yz} \\ \varepsilon_{xz} & \varepsilon_{yz} & \varepsilon_z \end{matrix} \tag{30}$$

The stress-strain relationship is contingent on the idea that the stress in a material can be described by the symmetric stress tensor as:

$$\sigma = \begin{matrix} \sigma_x & \tau_{xy} & \tau_{xz} \\ \tau_{yx} & \sigma_y & \tau_{yz} \\ \tau_{zx} & \tau_{zy} & \sigma_z \end{matrix} \tag{31}$$

where $\tau_{xy}=\tau_{yx}$, $\tau_{xz}=\tau_{zx}$, and $\tau_{yz}=\tau_{zy}$. The three normal stresses, σ_x, σ_y, and σ_z, and six shear stresses describe the stress in the material. If symmetry is used the six shear stresses can be reduced to three as shown above. In the COMSOL environment, the stress-strain relationship for a linear condition, such as the uniaxial loading of the absolute stent, is given by $\sigma = D\varepsilon$, where D is the 6x6 elasticity matrix, and the stress and strain components can be described in vector form as the following column vectors:

$$\sigma = \begin{matrix} \sigma_x \\ \sigma_y \\ \sigma_z \\ \tau_{xy} \\ \tau_{yz} \\ \tau_{xz} \end{matrix}, \varepsilon = \begin{matrix} \varepsilon_x \\ \varepsilon_y \\ \varepsilon_z \\ \gamma_{xy} \\ \gamma_{yz} \\ \gamma_{xz} \end{matrix} \tag{32}$$

The elasticity matrix D, or the simpler flexibility or compliance matrix D^{-1} is defined for isotropic, orthotropic, and anisotropic materials. For this investigation the Nitinol work-material is assumed to be an isotropic material; as such, the D^{-1} is inherently defined in the COMSOL structural mechanics branch as follows:

$$D^{-1} = \frac{1}{E}\begin{matrix} 1 & -\nu & -\nu & 0 & 0 & 0 \\ -\nu & 1 & -\nu & 0 & 0 & 0 \\ -\nu & -\nu & 1 & 0 & 0 & 0 \\ 0 & 0 & 0 & 2(1+\nu) & 0 & 0 \\ 0 & 0 & 0 & 0 & 2(1+\nu) & 0 \\ 0 & 0 & 0 & 0 & 0 & 2(1+\nu) \end{matrix} \tag{33}$$

In the above 6x6 matrix E is the modulus of elasticity, and ν is Poisson's ratio, which defines the contraction in the perpendicular direction. Inverting D^{-1} results in the elasticity matrix, D, as follows:

$$D = \frac{E}{(1+\nu)(1-2\nu)}\begin{bmatrix} 1-\nu & \nu & \nu & 0 & 0 & 0 \\ \nu & 1-\nu & \nu & 0 & 0 & 0 \\ \nu & \nu & 1-\nu & 0 & 0 & 0 \\ 0 & 0 & 0 & \frac{1-2\nu}{2} & 0 & 0 \\ 0 & 0 & 0 & 0 & \frac{1-2\nu}{2} & 0 \\ 0 & 0 & 0 & 0 & 0 & \frac{1-2\nu}{2} \end{bmatrix} \tag{34}$$

The implementation of the structural mechanics application mode is based on a weak formulation of the equilibrium equations in COMSOL Multiphysics. The weak form of the

equilibrium equations are expressed in the global stress components. Thus, the equilibrium equations expressed in the stresses for three dimensions are given as follows:

$$F_x = -\frac{\delta\sigma_x}{\delta x} - \frac{\delta\tau_{xy}}{\delta y} - \frac{\delta\tau_{xz}}{\delta z}, \quad F_y = -\frac{\delta\tau_{xy}}{\delta x} - \frac{\delta\sigma_y}{\delta y} - \frac{\delta\tau_{yz}}{\delta z},$$
$$F_z = -\frac{\delta\tau_{xz}}{\delta x} - \frac{\delta\tau_{yz}}{\delta y} - \frac{\delta\sigma_z}{\delta z} \qquad (35)$$

Here **F** represents the body forces acting on the Absolute stent geometry, and the expanded form can be condensed to the following relationship, $-\nabla \cdot \sigma = \boldsymbol{F}$. The aforementioned stress-strain and strain-displacement relationships can be substituted in the condensed equation, above, to yield the Navier's equation expressed in the displacement. Depending upon the selection of the application mode, i.e., static or transient, COMSOL solves the same equation, with a different solver.

For static analyses, as conducted in this study, substitution of the stress-strain and strain-displacement relationships into the static equilibrium equation results in the following Navier's equation of equilibrium, $-\nabla \cdot (c\nabla \boldsymbol{u}) = \boldsymbol{F}$. For the transient problem, introduction of Newton's Second Law yields the following equation for **F**:

$$\rho \frac{\delta^2 \boldsymbol{u}}{\delta t^2} - \nabla \cdot c\nabla \boldsymbol{u} = \boldsymbol{F} \qquad (36)$$

The structural mechanics module in conjunction with the mathematics module, used for the definition of the material behavior in terms of the Helmholtz free energy, defines the tensile and contraction loading scenarios evaluated in this study. Solving the inherent equations of the structural mechanics module with the prescribed set of ordinary differential equations that define the Nitinol will yield a theoretical solution that predicts the maximum displacement of the stent under an applied uniaxial loading.

2.5. Finite element simulation

2.5.1. FEM techniques

The two major challenges in this research were developing appropriate simulation parameters to minimize the computation time, and developing the model for the Nitinol work material. Initially the material properties of Steel AISI 4340 were chosen as a starting point to get the model running. Although no steel stents were experimentally tested, the theoretical deformation of the Absolute stent with the predefined steel work-material is beneficial in determining an initial envelope of theoretical parameters that can be processed by the COMSOL software. The four different stent lengths were tested to determine whether length of the stent played a role in the computation time for solutions. Furthermore, the mesh density was varied from the extremely coarse (few mesh elements) to normal, to determine whether this simulation parameter has an effect on the computation time. Thus, use of the steel material allowed for the determination of appropriate simulation parameters that are used to minimize the computation time necessary to determine the behavior of the Nitinol.

A modular approach was taken in creating the Nitinol material model. A simple model was initially created and then modified to ensure that the material phase change is accurately represented. As such, three different models of increasing complexity were created. These are discussed in the following section. The envelope of the simulation parameters determined from the Steel AISI 4340 was used in conjunction with each of the three Nitinol models to determine the efficacy of each one.

A stationary solver was used for all the simulations in this investigation. The stationary solver is an implicit one that is useful in solving for the global response of the stent structure to an applied load. The implicit solver finds solutions to all linear equations from all time steps simultaneously. An explicit solver is useful for looking at the local response of a system to an applied load that lasts for a short period of time. Thus, the implicit solver has a linear approximation step that forces equilibrium. The stationary study feature in COMSOL corresponds to a stationary solver (default), a parametric solver, or an optimization solver. This solver is intended for a steady-state situation, and all time derivatives are ignored. This is used to aid in the description of the mechanical response of the Absolute Guidant stent of different lengths to uniaxial loading conditions.

2.5.2. Model parameters and material properties

Figure 2.4 shows the constraints and loads on a 14.42 mm stent. One end of the stent was fixed in every direction, while a uniaxial tensile load was applied in the z-direction to the other end (along the axis of the stent), keeping the stent fixed in x- and y-directions.

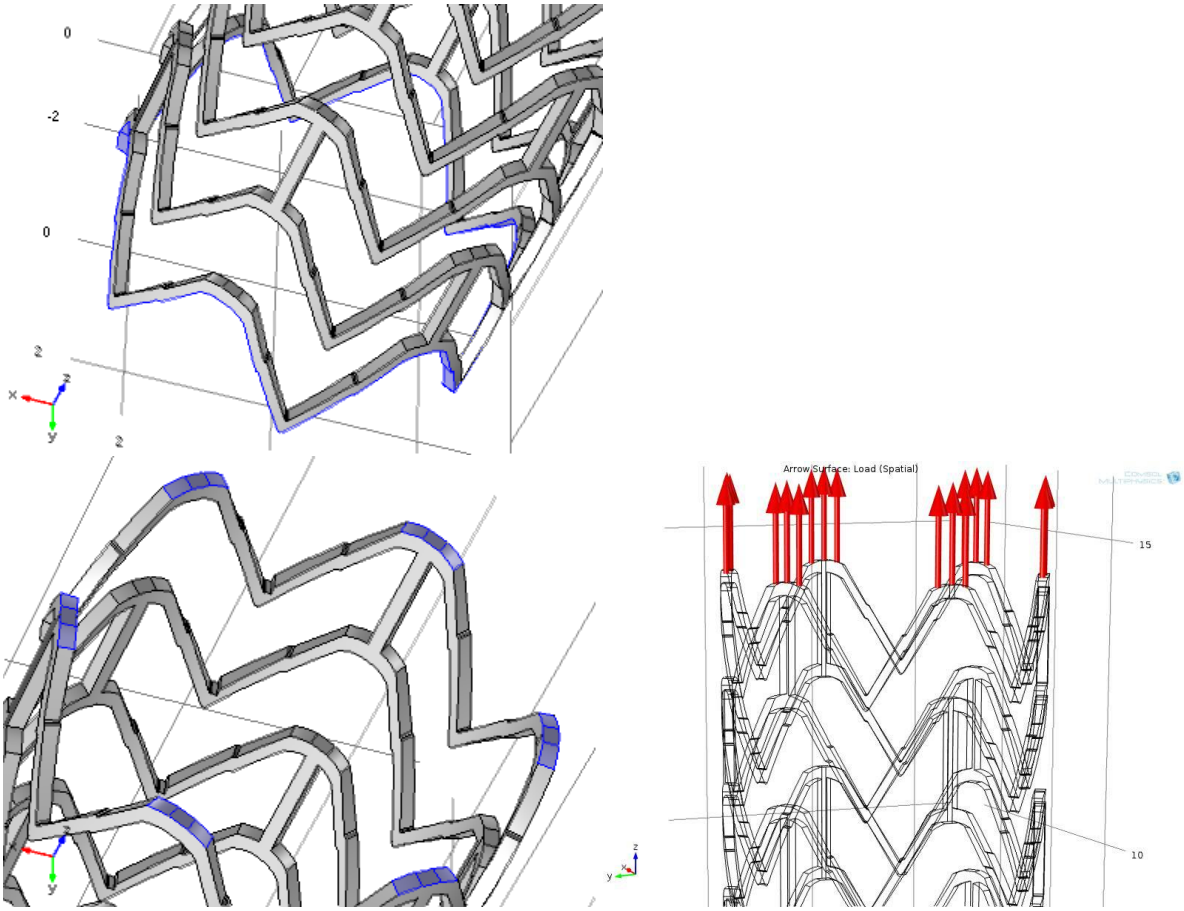

Figure 2.4 Constraints (right) and Load (left) boundary conditions

All static loading simulations were carried out in this manner, with different applied loads chosen to reflect the loading scenarios from the experimental tensile tests of the stent specimen. The loading area was 2.0331×10^{-8} m^2. The uniaxial boundary loads were applied in the z-direction, while fixing the displacement of the stent in the x- and y-directions. The mesh density was varied five different times, from extremely coarse (4,774 elements) to normal (33,208 elements), to determine whether the theoretical solution is dependent on the element size. Figure 2.5 shows a sample of the mesh generation in the COMSOL work environment. The 10.87 and

21.54 mm stents were also tested for the same range of element sizes (mesh density). Figure 2.6 plots the percent strain as a function of the number of mesh elements.

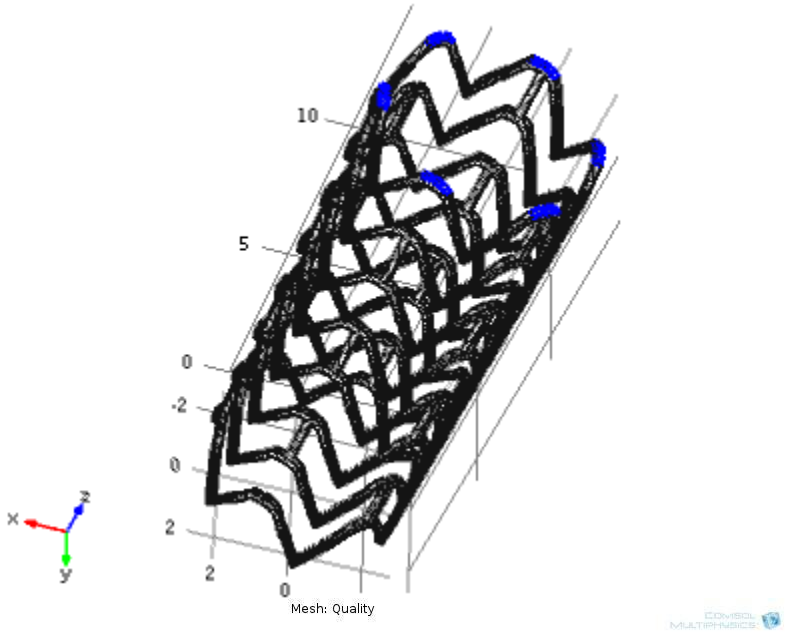

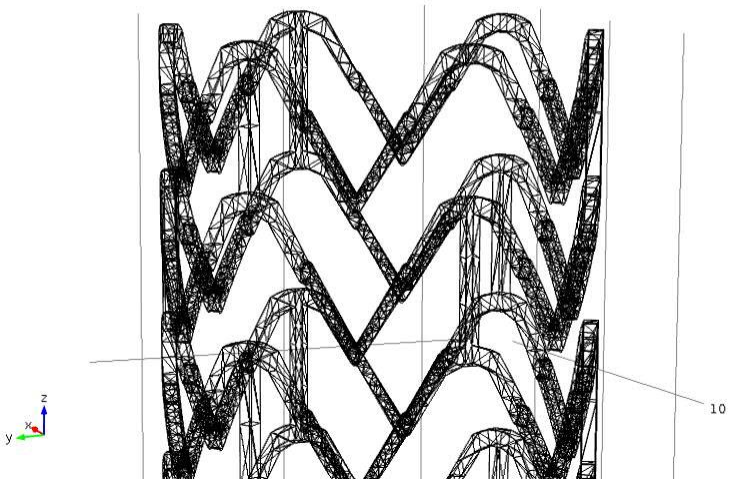

Fig 2.5 Mesh for 14.42 mm stent

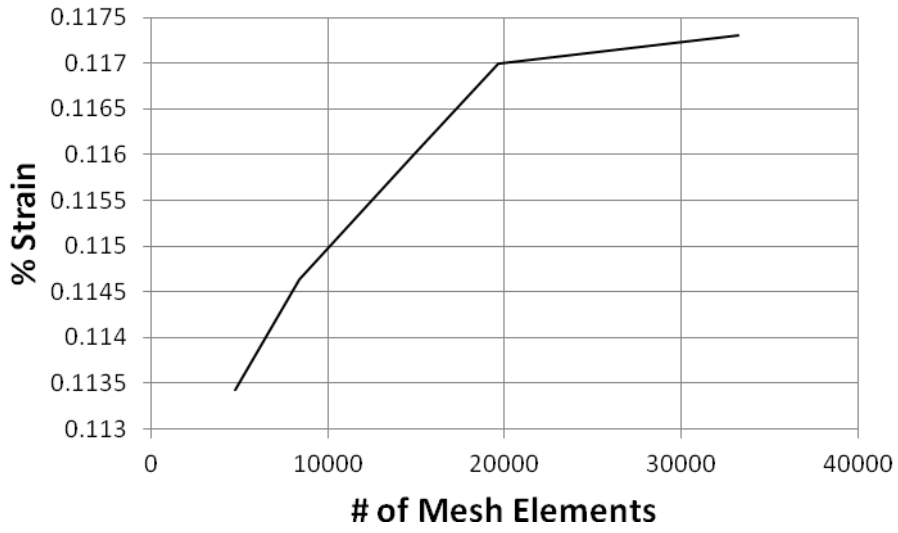

Figure 2.6: Mesh Sensitivity for 7.30 mm stent

For a step change in mesh density, for the same applied force of 0.04 N, there is less than a 1.5% change in the predicted elongation of the stent. It also shows the same elongation versus number of mesh elements for the 7.30 mm stent with the material properties for Nitinol defined. According to Fig. 2.6, there is a $\leq$ 1% change in the predicted strain if the mesh density is changed for simulations with Nitinol, so it is assumed that the mesh density has a negligible effect on the results, and subsequent simulations were done at a mesh density that minimizes computation time.

As the length of the modeled stent increased, the computation time increased. At a high mesh density, it is likely that solution time would exceed any practical research purpose. Thus, for the three different stent lengths of the same (Absolute) geometry, the calculated strain is considered to be independent of the number of mesh elements at higher mesh densities. From the elongation-mesh density relation, it becomes evident that at higher mesh densities the percent change of the elongation with respect to the element number is closer to 0.25% indicating that future simulations be done while attempting to strike a balance between the number of elements in the mesh and the computation time. It is important to note that the solution time did increase with increasing stent length from approximately 8 s for the 7.30 mm stent to several hours for the 14.42 mm stent.

2.6. Investigation of model parameters

The initial tests of the Absolute geometry as a steel stent revealed several pertinent details related to the envelope of simulation parameters. These are presented here followed by a discussion of the three different Nitinol material models, the results of, which, are discussed in the subsequent sections. COMSOL affords users an extensive material library from which selections can be made. Steel AISI 4340 is one such material, and was selected as a precursor to the actual Nitinol work material. The basis for selection depended on the fact that several stents are made using medical grade steel, and although the predefined material from the COMSOL library is not exactly the same, it was assumed that the behavior of these two different steel alloys would not demonstrate significant changes as related to the deformation behavior of the Absolute stent geometry. Table 2.1 presents the material properties of the Steel AISI 4340.

Table 2.1: Steel AISI 4340 Properties

Property	Value	
Density	7850	[kg/m^3]
Young's Modulus	2.05E+11	[Pa]
Poisson's Ratio	0.28	[1]
Thermal Coefficient	1.23E-05	[1/K]

Once the solution dependence on the mesh density, and the stent length was determined, an envelope of simulation parameters was set, and the Nitinol material model was implemented next. The initial Nitinol model was simple and based on the specification of material properties. In the COMSOL environment, users can either select from a predefined library of materials, or specify material properties themselves. Young's modulus, Poisson's ratio, and the density were defined for the Nitinol work material and are presented in Table 2.2. These values were taken from Petrini et al. [2005] and Ghosh et al. [2011].

Table 2.2: Nitinol Material Properties (Simple Model)

Nitinol Material Properties (Simple Model)			
Y	Elastic (Young's Modulus)	7.50E+10	[Pa]
ν	Poisson's Ratio	0.3	[1]

ρ	Density	6478 [kg/m^3]

These values were input to define the material. The same isotropic linear elastic material model was selected as was done previously for the steel. No accommodations for the plasticity or the characteristic phase change that Nitinol undergoes were made. The structural mechanics module in the COMSOL software calculated the elongation of the Absolute stent geometry for various applied loads. The load (N/m^2) was applied to the same loading area, and the results plotted to get a working Nitinol material model before using the thermodynamic potential to create a more complicated material description to be solved alongside the inherent continuum mechanics equations. Tension and contraction loadings were carried out for the 7.30 and 10.87 mm stents. The same mesh density was used for both lengths, and comprised of 60,478 tetrahedral elements. The extension/length is plotted as a function of the applied load for both stents and the results are presented in Fig. 2.7.

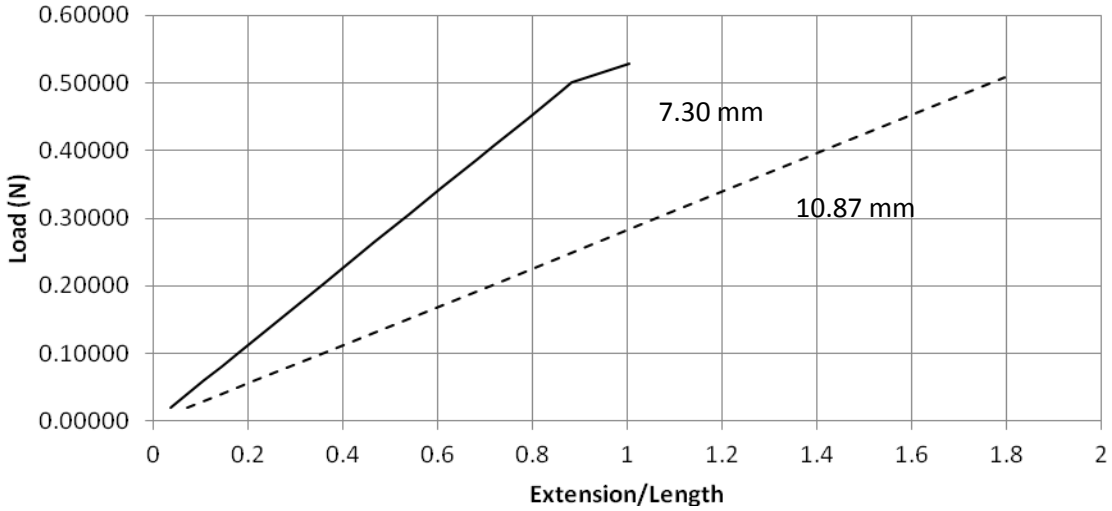

Figure 2.7: Nitinol Absolute Stent 7.30 mm (solid), and 10.87 mm (dashed) Tensile Loadings

The simple Nitinol material model for the 7.30 and 10.87 mm stents shows the linear elastic region of the Nitinol Absolute stent deformation to various tensile loads. The lines have different slope, and can be understood if one considers that the longer 10.87 mm stent would be expected to be less stiff than the shorter 7.30 mm stent. Thus, the slope of the elastic region would be

"flatter" than that of the more rigid stent. From the 7.30 mm plot it seems, that the load at which the Nitinol work-material begins to undergo the phase change from the parent austenite to the martensite phase when the extension is equal to the original stent length. This is not as evident in the plot for the 10.87 mm stent, even though the initial linear elastic region is clearly defined. Compared to the steel 7.30 mm stent, it becomes evident that, as expected, for the same applied load the Nitinol work-material exhibits a much large deformation than does the steel. Contraction loadings for the 7.30 mm and 10.87 mm stents were also carried out. The results of these are not graphically presented as the COMSOL software simply predicted that the response to a uniaxial contraction applied load as the same as the tensile loadings, but in the opposite direction.

With these initial results in hand, especially the model parameters, a more complicated material model was constructed that introduced plasticity, and a transformation function based on the thermodynamic potential to describe the forward phase change that the Nitinol undergoes when a tensile or contraction load is applied. Based on the model built by Petrini et al. [2005], and Lagoudas [2008] the plasticity conditions for the Nitinol work material were first defined. In addition to the material properties presented in Table 2.2, the plasticity characteristics of the Nitinol were defined in accordance with Fig. 2.2. The global parameters defined for this material model are presented in Table 2.3.

Table 2.3: Material Properties of Nitinol

E	Elastic Modulus	7.50E+10	Pa
v	Poisson's Ratio	0.3	[1]
ϵ_L	Transformation strain	0.07	[1]
h	Transformation phase tangent modulus	4.00E+09	Pa
β	Coefficient of stress deviatoric component inducing transformation-temperature relation	7.00E+06	Pa/K
M_f	Martensite finish temperature	263	K
T	Current temperature	292	K
R	Half of the mechanical hysteresis loop amplitude in uniaxial tension-compression case	7.00E+07	Pa
m	Coefficient related to the asymmetric behavior of Nitinol in tension and compression	0	[1]

According to Fig. 2.3, the stress at which phase transformation within the Nitinol work-material starts to occur can be considered to be the yield stress input in the COMSOL environment. In addition to the linear elastic material model, an isotropic hardening curve is designated, for which the phase tangent modulus is assumed to be the slope. With these inputs

defining the points at which one would expect forward transformation to occur, Absolute stents of lengths 7.30, 10.87, and 14.42 mm were tested. Figure 2.8 shows how the strain (extension/length) is related to the applied load for the 7.30 mm stent.

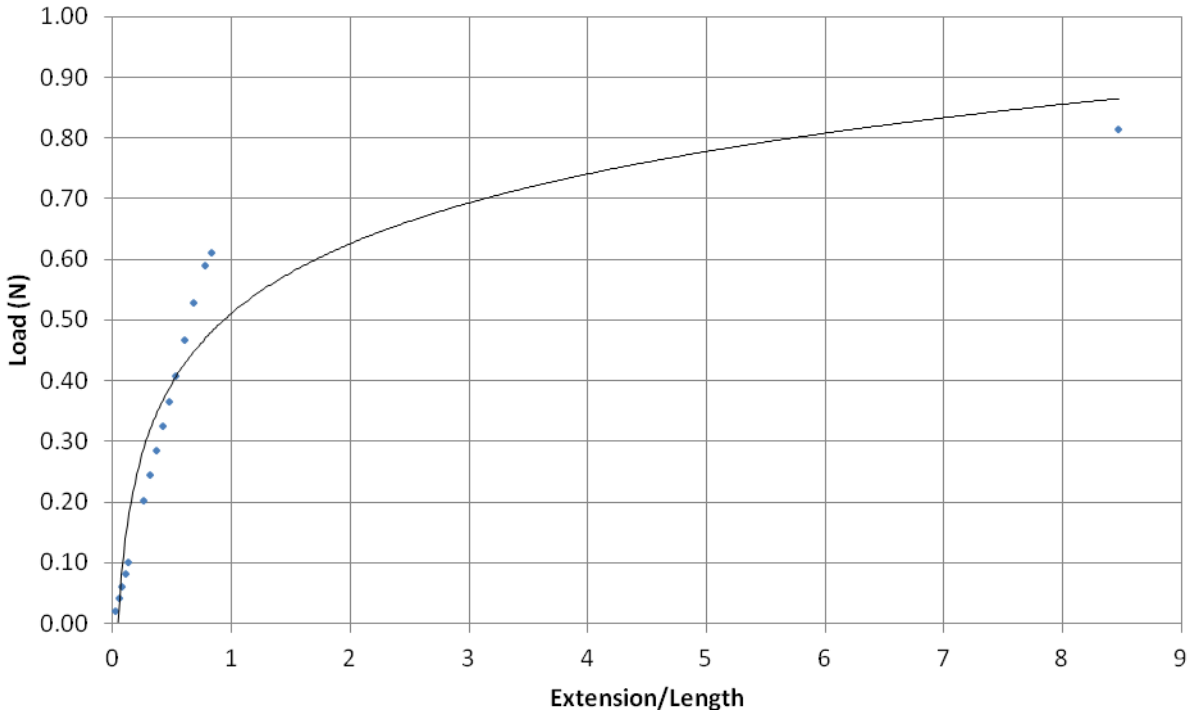

Figure 2.8: Load vs. Strain 7.30 mm

A logarithmic curve was fit to the data, which exhibits an initial linear elastic region, followed by a region that represents the phase change the Nitinol work material is undergoing. It appears that for this stent length, the load at which phase transformation would occur is between 0.6 and 0.7 N. The COMSOL software also provided the max von Mises stress occurring at any part of the Absolute stent. The max von Mises stress associated with each load is plotted against the strain, and is presented in Fig. 2.9 for all three simulated stents.

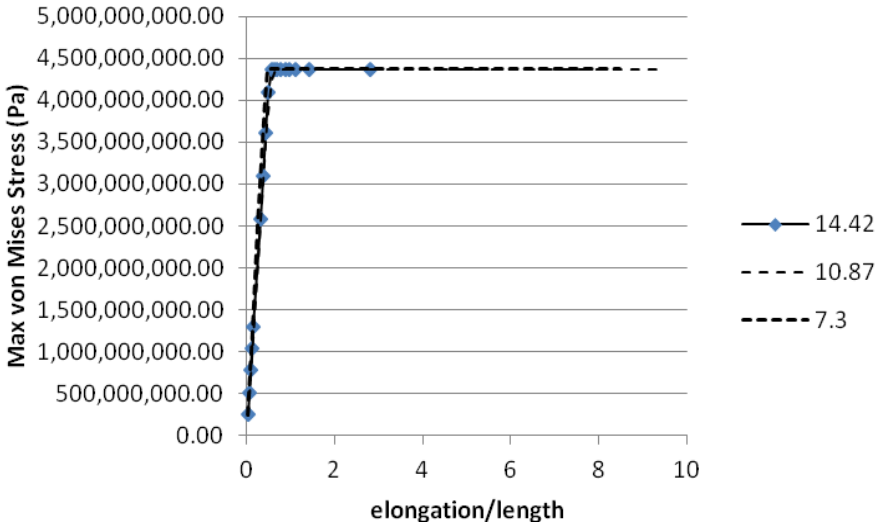

Figure 2.9: Stress-Strain for Three Simulated Stents

From Fig. 2.9 it becomes evident that at 4.5×10^9 Pa, increasing the load, and thereby the elongation of the stent under a uniaxial tensile load, does not affect the induced stress in the stent geometry. This can be explained as a material parameter, i.e., the characteristic phase change of the Nitinol under applied stress, or as a result of the stent geometry. It is likely that the stent geometry adjusts to accommodate for the applied load, which can be distributed through the struts and bridges of the 7.30 mm absolute stent in order to ensure structural integrity. It is likely that the physical response of the stent is a combination of the two.

Figure 2.10 shows the load-strain curve as Fig. 2.9, but for the 10.87 mm stent.

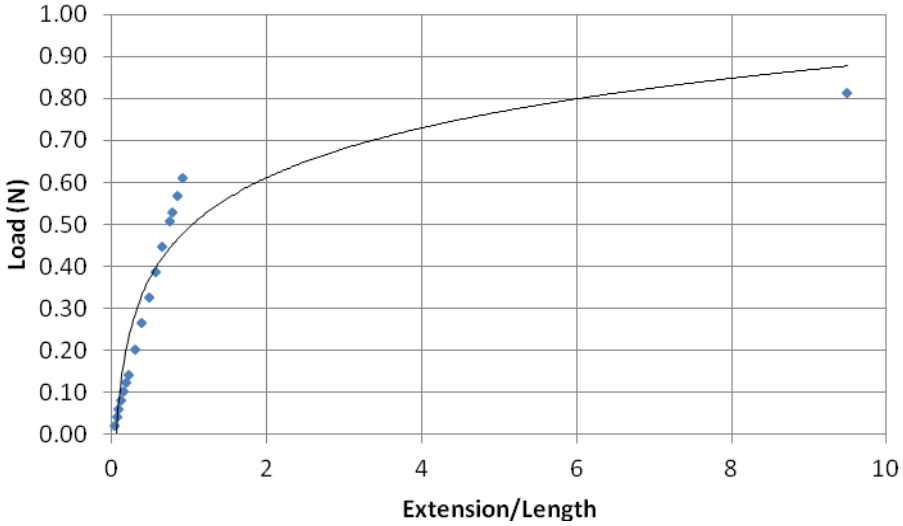

Figure 2.10: Load-Strain 10.87 mm

A similar relationship is acquired for the 10.87 mm stent, with the phase change plateau again occurring between 0.6 and 0.7 N. Figure 2.9 shows the stress strain relation for the 10.87 mm stent, and it is evident that the max von Mises stress experienced by the stent under tensile loading conditions is again approximately 4.5×10^9 Pa.

Figure 2.11 shows the load-elongation curve for the 14.42 mm stent. Fig. 2.9 shows the

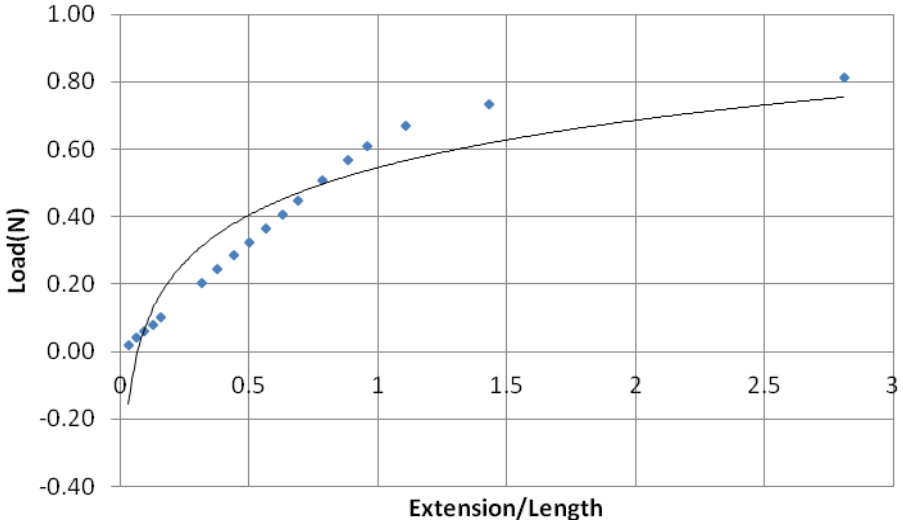

Figure 2.11: Load-Strain for 14.42 mm

stress-strain relation for this length as well. The same values for the load at which the Nitinol work-material undergoes a phase change, and the maximum von Mises stress induced due to loading. This is characteristic of what is discovered in literature, as the Nitinol displays the characteristic plateau during which added external uniaxial stress leads to very little stress generation within the material, but creates large deformations. Fig. 2.12 shows a plot of all three load-strain relations for the stents of different lengths.

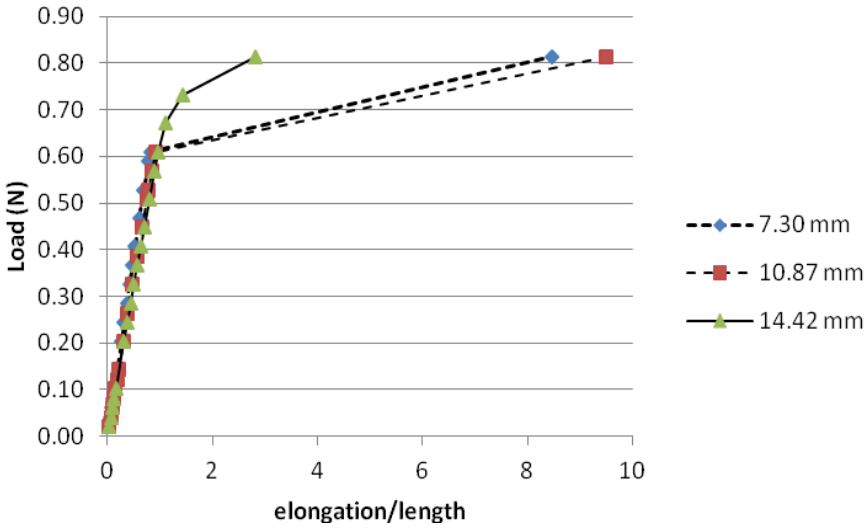

Figure 1.12: Comparison of Theoretical Load-Strain

2.7. FEM analysis of work-material deformation and stress

A von Mises stress distribution is shown in Fig. 2.13 for the 10.87 mm stent in response to a 0.203 N uniaxial tensile load.

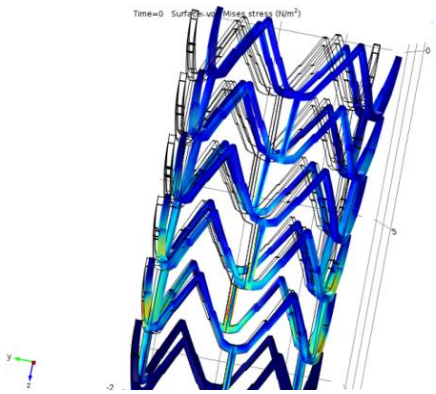

Figure 2.13: von Mises stress distribution for 10.87 mm stent

The stress appears to be concentrated near the struts linking each individual bridge. However, the stent does not appear to be fixed in the x- and y- directions. This was addressed in the future simulations with the more descriptive material model for Nitinol.

The advantage of FEM simulation is the ability to gain insight into the stent deformation, strain, and stress profiles, which are difficult to measure experimentally. Moreover, it is easy to visualize the location of stress concentration using the COMSOL visual output. Figure 2.14 shows the maximum von Mises stress induced in each of the three stents tested. The applied load, 40×10^6 N/m^2, was applied to an area of 2.0331×10^{-8} m^2. This translated to a 0.813 N load. It is evident from the images that much of the stress is concentrated in the strut-bridge connection region. Based on this one would expect that these linkages would see structural failure before. It is likely that at loads above 1 N, the struts connecting the bridges would start to fail and, thus, compromise the stent geometry.

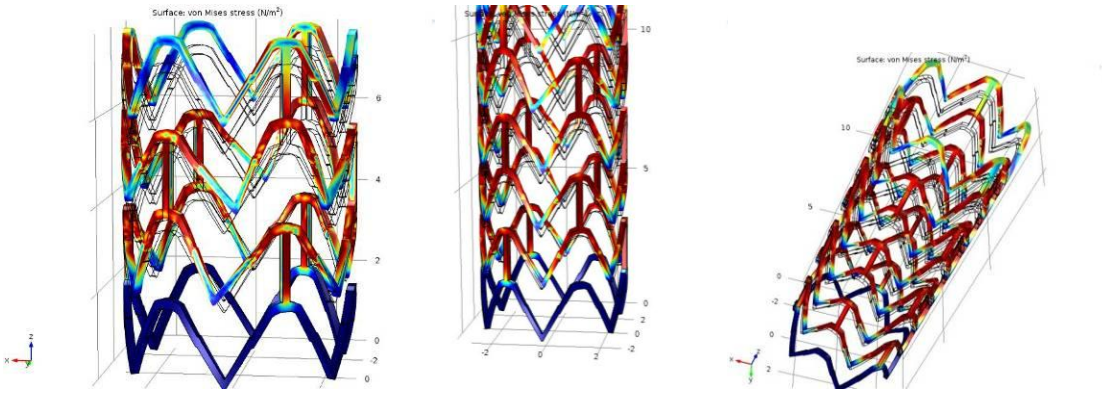

Figure 2.14: von Mises Stress Distribution for 7.30 (top left), 10.87 (top right) and 14.42 mm stents

The figure above shows that at loads close to 1 N one might expect the stent structure to fail. This is indicated by the high stress locations near the strut-bridge connections.

2.8. Conclusions

There are several important conclusions to draw from the above simulations. First, an envelope of parameters was created in which several modeling guidelines were set to strike a balance between the computation time and the mesh density as well as the length of the stent. It was qualitatively observed that increasing the length of the stent increased computation time. As such the mesh density became an important parameter. Since it is possible to find a solution for a longer stent at a coarser mesh density (less elements, larger elements), the dependence of the

solution on the element size was determined. It was found that the element size affects the predicted solution by $\leq 1\%$. This was first determined using the simple Steel AISI 4340 from the COMSOL material library, and then verified with the Nitinol material model. Three different stent lengths, 7.30, 10.87, and 14.42 mm were tested given Nitinol work-material. Each stent was subject to 15 to 20 static loading conditions, where one end of the stent was fixed and the other end had an applied boundary load. The elongation and maximum von Mises stress for each uniaxial static loading was recorded, and used to generate load-strain, and stress-strain plots for each of the three tested stents. From here it was discovered, that the COMSOL software predicted the load at which one could expect phase transformation to occur as 0.6 to 0.7 N. Moreover, from the stress-strain plots, the maximum von Mises stress incurred was on the order of 4.5×10^9 Pa. The model output can give more detailed information than is possible from experimental analysis. The modeling results show stress distribution throughout the stent and regions of high stress and strain concentrations.

Chapter 3: Experimental Analysis of Absolute Stent

3.1. Introduction

Experimental measurements of stent deformation and strength properties are necessary as a basis for validation of the theoretical forced responses output by the FEM software. These results are imperative in determining the efficacy of the CAD and material models. Close relation between the theoretical model and the experimental results would afford the researcher an opportunity to theoretically test the forced responses of proposed stent designs prior to manufacture with a high degree of confidence in the expected results. The testing methods employed in this chapter are in line with those presented in the American Society for Testing and Materials (ASTM). In addition to the characterization of stents according to ASTM standards, other tests for determining stent properties are presented here.

ASTM provides a standard guide for the characterization and presentation of the dimensional attributes of vascular stents. These are reviewed as a precursor to the experimental procedures carried out in this investigation. Although there are significant differences between BE and SE stents that stem from the material properties, many of the dimensional attributes are common and worth reviewing in a comparative manner. The ASTM guide addresses the dimensional characteristics of stents irrespective of the material properties and stent functional characteristics [ASTM, 2009]. All the dimensional characteristics are presented for *in vitro* conditions with knowledge that *in vivo* characteristics are patient specific, and may be slightly different. It is important to note that the ASTM dimensional characterizations are not for stents intended for placement in nonvascular regions like the esophagus, and bile duct, but can be used for such locations as well.

Any *in vivo* mechanical loadings must be considered when designing a stent for implantation. Thus, the reaction of individual struts, and the bridges connecting these struts to forced loading becomes important. Changes in the diameter and length of the stent due to internal pressure, tensile, compressive, torsional, and bending type loads become paramount design criteria when developing new stents or attempting to improve the long-term patency of pre-existing stent geometries. This study focuses on some standard *in vitro* mechanical loading tests in congruence with the methodologies prescribed by ASTM. The dimensional attributes included in the ASTM guide are those deemed to be predictive of successful clinical performance. However, given the

myriad of patient and medical factors in any stent implantation (angioplasty) procedure, the clinical outcome cannot be solely based on the ASTM recommendations for the clinically relevant dimensions. Thus, *in vitro* testing of stents can be used as a barometer for simulated *in vivo* conditions.

Experimental testing of stents is the dominant mode for determining whether a specific stent geometry of a particular material can withstand *in vitro* and *in vivo* loading. Most stent geometries are subject to various *in vitro* mechanical loadings to determine their responses to forced loading. BE and SE stents may be subject to such testing protocol outlined for metals and metal alloys. The ASTM test methods are "valid for determining stent failure due to typical cyclic blood vessel diametric distension" [ASTM, 2009]. However, it is important to note that these test methods do not address other modes of failure due to dynamic bending, torsion, extension, crushing, or abrasion. Pulsatile loading was neither modeled, nor was it explored experimentally in this investigation. The importance, of such tests is, nonetheless, important for future considerations, as much of the standard testing methodology keys on the BE stent type with little or no attention paid to failure characterization of SE stents.

3.2. Literature Review

In order to have a basis for comparison for the theoretical loadings of the absolute stent simple experimental tests were designed. These tests were based on the ASTM standard method for tension testing of Nickel-Titanium (Nitinol) superelastic materials. The ASTM test method covers the tension testing of superelastic Nitinol materials. In particular these methods focus on the determination of the upper plateau strength, lower plateau strength, residual elongation, tensile strength, and elongation. Of these, elongation and tensile strength are of importance with respect to this investigation. Tension tests provide information on the superelasticity of the material in question.

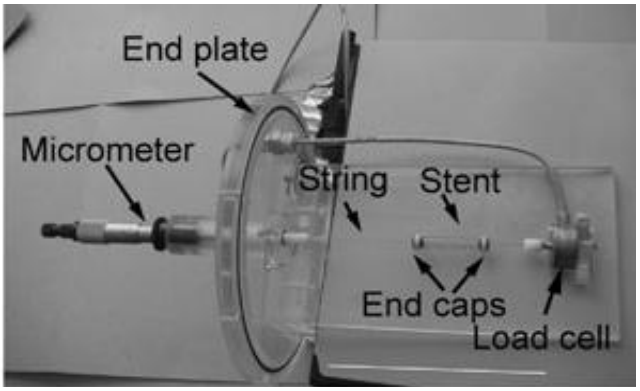

Fig. 3.2: Tension Device for Nitinol Stent Load [Simons et al. 2010]

Simons et al. [2010] studied the load deformation behavior of Nitinol stents in great detail. They devised testing devices to measure the loads in stents undergoing tensile, torsional, and bending deformations whereby the Nitinol stent of interest could be placed over two endcaps and held in place with plastic slip rings, as shown in Fig. 3.1. One endcap was attached with string to a load cell and other to a micrometer head that was fitted through the endplate. When the micrometer head was rotated the end of the stent was displaced and loaded the stent in tension with a measured force. From this study Simons and colleagues found that a linear relationship exists between axial strain and increasing load. They also found that in tension the struts tend to change shape dramatically and non-uniformly to accommodate the axial deformation. As was the case in the experiments presented in this investigation, the stents were deformed at air temperature, but Simons and colleagues deformed the stents plastically to study the deformation patterns.

Another relevant study focuses on the fatigue characteristics of Nitinol using the tension-tension method. Lin et al. [2011] investigated the Nitinol fatigue strain limit versus both strain amplitude and mean strain using the tension-tension method. The overall setup included load cells on each upper grip for the specimens that were put in tension. One significant result of these tests was the discovery that in tension-tension loading Nitinol has better fatigue resistance in its single phase than in its coexisting phases [Lin et al. 2011]. Using these tests as a reference, this investigation established the relationship between applied load and associated elongation (strain) for a given specimen of the Guidant Absolute Stent, and is presented in the following section.

3.3. Stent Property Experimental Measurements

Experimental force measurements were conducted for comparison to the simulated force response of the stent. A 100 mm long specimen of the Guidant Absolute Stent was used to experimentally measure the forces of interest. Tensile loading of the Guidant Absolute Stent was carried out using an INSTRON tension testing machine (model # 4206-004). As previously mentioned tension tests provide information on the strength and ductility of materials under uniaxial tensile stresses; they also provide information on the superelasticity of the material being tested. These tests were conducted to observe the stent response to an increasing

displacement, which is similar to the tensile loadings experienced during deployment procedures as well as stent and arterial wall interactions [Simons et al. 2010].

As part of this study, experiments were conducted at the University of Michigan (UM) to measure the contractile forced response of an Absolute Stent. Elongation and crush tests were performed, the results of which, are used for comparison in this investigation. The same 100 mm stent was used for these tests. For the contraction test, a stent was placed between the dynamometer and a fixed wall. One end of the stent was held in position with a clamp attached to the dynamometer, and the other end was placed over a short rod cantilevered from the fixed wall to prevent vertical slippage against the wall surface. The dynamometer was held at a control stage from which controlled displacements of the clamped end of the stent were made possible. Force measurements were recorded for displacements of 10, 15, and 20 mm, corresponding to contractions of 10%, 15%, and 20%, respectively, of the original stent length.

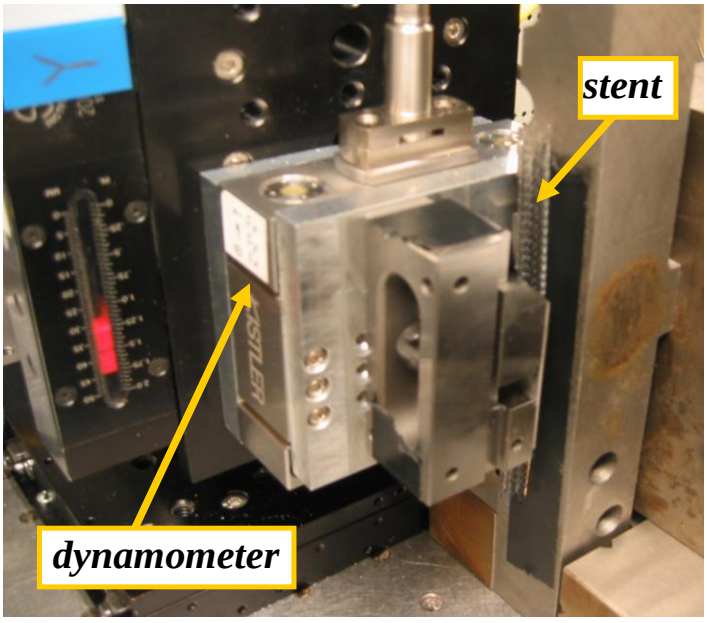

Fig. 3.2. Experimental setup of stent crush test

Crush tests were also conducted at UM, as shown in Fig. 3.2. These tests consisted of placing the stent vertically between the dynamometer and fixed wall, at which point, the dynamometer was moved toward the wall to crush the stent. Precautions were taken to minimize the initial force introduced to the system due to the stent's position between the dynamometer and the wall. Force measurements were again recorded for crush distances of 0.5, 1, 1.5, and 2 mm. These crush distances corresponded to 8.3%, 16.7%, 25%, and 33.3% of the original diameter crushed.

3.3.1. Experimental Setup and Procedure

The INSTRON 4000 series tension tester and the INSTRON 5500 series were adjusted with the appropriate load cells to study the stent response to tensile loading. A 100 N load cell was used and the Absolute Stent sample was loaded into the wedge action grips (Fig. 3.3). Tensile force and elongation were measured in the experiment. Tensile force was measured by a load cell, which is a transducer that converts tension into an electrical signal. Extension was measured by the encoder mounted in the INSTRON. A load was applied to the stent specimen via a moving crosshead.

Prior to loading into the wedge action grip two brackets were manufactured from scrap metal to insert into the stent (Fig. 3.3(b)). Since the stent specimen could not be directly loaded into the wedge grips these were necessary to fasten the specimen to and insert between the wedge grips. The cylindrical portion of the brackets had a diameter of 4 mm to ensure a snug fit into either end of the stent. The two cylindrical portions of each bracket was inserted into opposite ends of the stent and fastened with two zip-ties so that the bracket-stent connection would not come up apart during testing. Once the stent was mounted on the brackets, whose thickness was approximately 5 mm, the entire assembly could be mounted into the wedge grips of the INSTRON (Fig 3.3(a)). The grips can be tightened onto a specimen without altering the vertical position of the faces in relation to the specimen. This feature enabled the selection of the exact point at which the specimen was held. In this manner, the initial gage length did not change, and there was no compressive force applied, which may have led to buckling. Thus, a strong clamping force was applied to the specimen, which was difficult to hold, because of the mechanical advantage afforded by the tightening mechanism. Once the Absolute Stent

(a) (b)

Fig. 3.3 (a): Instron tensile tester (Google Images); (b) Stent mounted onto graspable adapter

specimen was loaded into the wedge grips and tightened, the tension test was carried out. The rate at which the stent was elongated was 10 mm/min at 50% humidity and a room temperature of 28^{o}C. There were 10 specimens per sample with two different samples for the test. The results from the tension tests are presented in the next section.

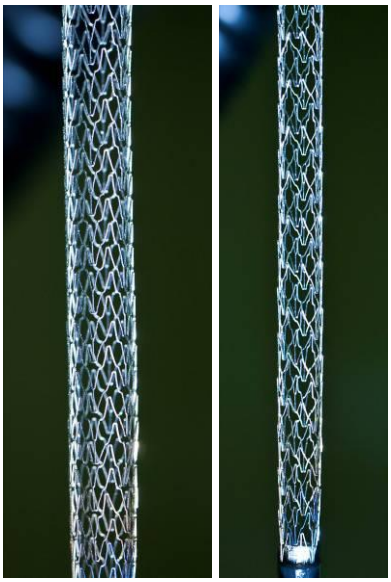

(a) unloaded **(b) loaded**

Fig. 3.4 Guidant Absolute Stent under different loading conditions

3.3.2. Results and Discussion

3.3.2.1. Elastic Deformation

Figure 3.4 shows the stent deformation from tensile loading. Figure 3.4 (a) shows the stent with no applied load and Fig. 3.4 (b) shows the same stent under approximately 0.6 N. The mode of elongation is evidenced by these figures and it is interesting to note that the bridges between stents alternated directions when being subjected to a load, i.e., one bridge turned left while the subsequent one went to the right, for the entire length of the stent. It is plausible that because of this alternating pattern the Guidant Absolute Stent can recover nearly 20% strain upon unloading.

Figure 3.5 relates the elongation of the stent to the applied load. The tensile stress at maximum load (0.64 N) was 0.02 MPa, and test the tensile strain was 77.31%, but upon release the stent returned to its original length due to the superelastic property of the Nitinol. Multiple tensile tests were performed with different load cells (100 N and 250 N maximum load) with identical results.

From Fig. 3.5 it becomes evident that there exists a linear relationship between the elongation and the applied load. The % strain was calculated as a ratio of the extension to the original length of the absolute stent (105 mm). Once the tensile loading was removed the stent returned to its original length with no plastic deformation. These deformations in the elastic region of Nitinol verfiy the ability of the material to undergo significant loading in the axial direction and still maintain the original shape.

The data generated by the 250 N load cell was very similar to that obtained using the 100 N load cell, but the resolution of the data with the 250 N load cell was less precise. Accuracy for

the 100 N load cell is equal to or better than 0.025% of the load cell rated output or 0.25% of the indicated load. The maximum measured forces are approximately 4% of the 100 N maximum load. Regardless of the resolution, the same linear relationship exists as demonstrated by the first set of experiments (Fig. 3.5). The experimental data represent the elastic region of the shape memory alloy NiTi, and demonstrate that the material can recover nearly 18% strain, which makes it more suitable for implantation into arterial lesions that experience unique mechanical stresses. This also affirms the notion that shape memory alloys such as NiTi are more suitable for in vivo applications as they more aptly mimic the elasticity of human tissue.

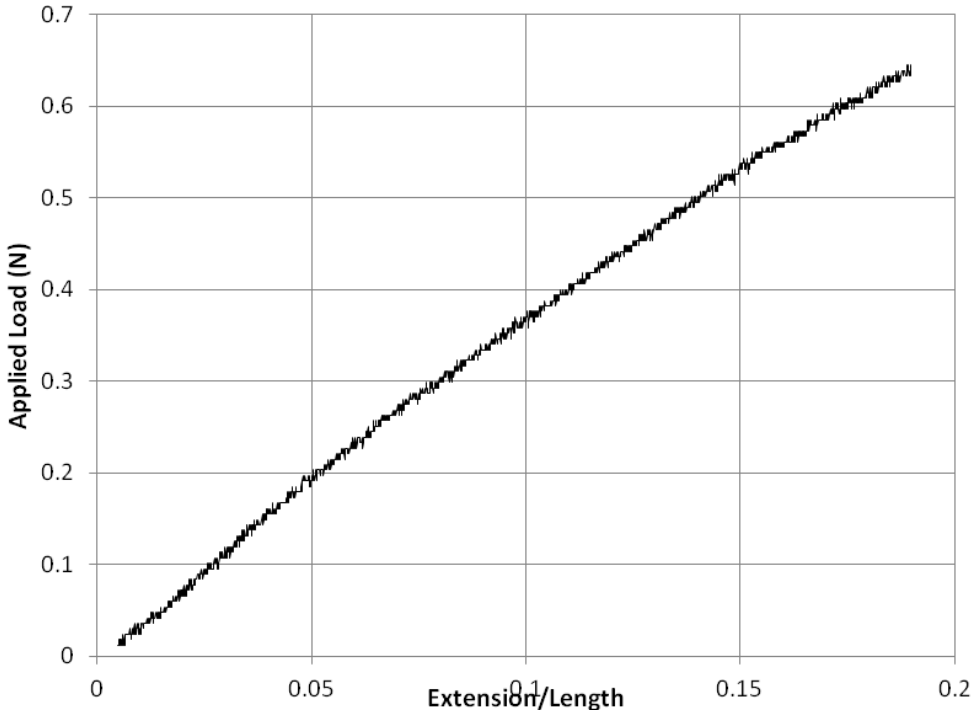

Fig. 3.5: Applied Load versus Extension/Length (100 N Load Cell)

3.3.2.1. Large Deformation: Tensile Test to Fracture

Figure 3.6 shows images of large deformation of the stent, and Fig. 3.7 shows the applied load versus extension/length for a tensile test using the 100 N load cell. The stent was elongated in this test at the same 10 mm/min, but was loaded beyond the ultimate tensile stress, at which point the stent fractured. There was a plateau from approximately 45% strain to 140% strain. One of the bridges was observed to break at approximately 180% strain, which correlates to the

drop in load in the graph. The “steeper” increase from the end of the initial plateau continued until the second broken bridge, which was characterized by a larger “spike”, and associated drop in force. Immediately after the second bridge broke, another break followed, as shown by the force drop just before 250% strain. At this point the stent continued to elongate under the tensile loading, until the zip-tie grips slipped off the stent end.

The large deformation of the stent subjected to increasing tensile loads can best be understood as a function of the stent geometry as well as the material properties. Although Nitinol wires can only recover at most 10% strain, a Nitinol structure can be expected to handle strains much greater than a simple wire. The elastic tests were stopped at approximately 20% strain in order to preserve the specimen for future testing. It becomes evident with this final tension test that the linear relationship is, indeed, upheld for loads up to 0.8 N. One can assume that beyond this point, in the plateau region, the specimen geometry allows for a significant increase in the deformation, with a minimal increase in the force. However, when the stent undergoes large deformation and the wires of the stent align in the direction of the force, the applied load increases more rapidly and bridge elements between struts begin to break. Thus, it is plausible that the plateau region results from the specimen geometry and any further deformation results from a combination of geometry and material effects. Although complete stent fracture (breaking of all bridge elements) was not witnessed due to the experimental setup, one could expect similar spikes at bridge break points. The images in Fig. 3.6 were taken at different points in the tension test to fracture.

Figure 3.8 shows the experimental results obtained for the stent contraction tests conducted at the University of Michigan. From these results it becomes evident that repeating the experimental results with a dedicated stent fixture would lead to more reliable data points. Furthermore, repeating the experiment several times could also lead to more reliable data that affords opportunities to make significant conclusions. From comparison to figure 3.5, it becomes evident that less force is needed to shorten the stent longitudinally than is needed to elongate it in the reverse direction. It is likely that the stent design accounts for the location of implant, as it is more likely to be under contraction loadings rather than tensile in the popliteal segment. Thus, the stent must needs to contract more readily than it needs to elongate.

Figure 3.6: Images of Deformed Absolute Stent

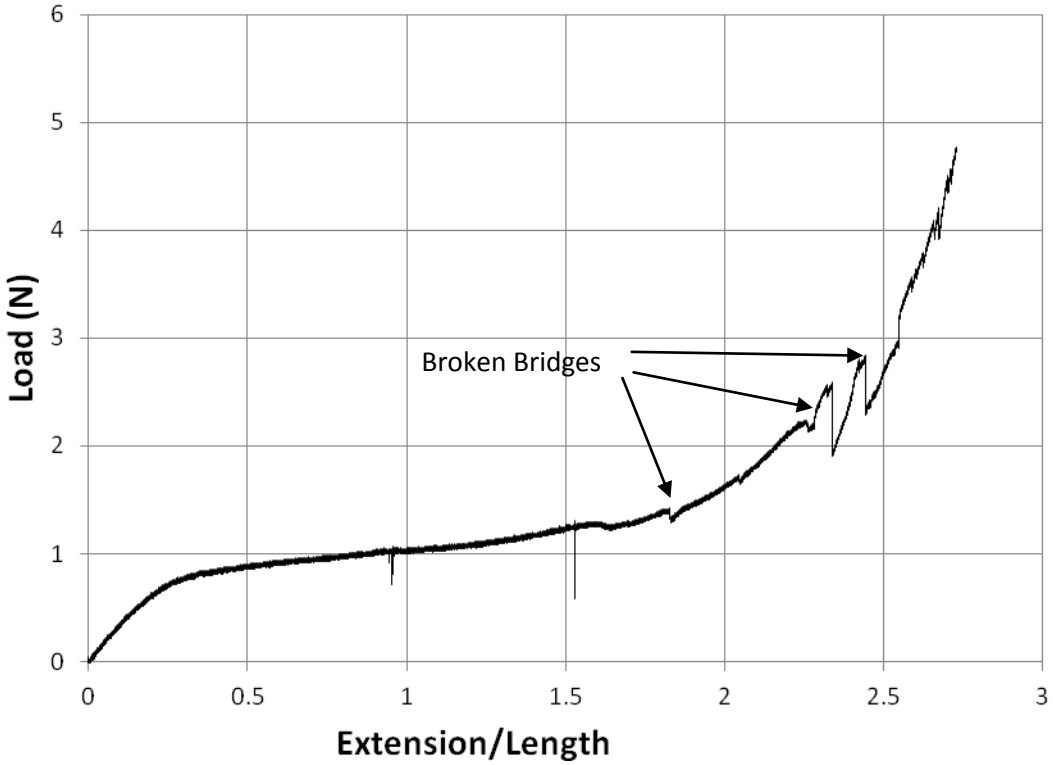

Figure 3.7: Tension Test till Stent Fracture

Figure 3.8 shows the experimental results obtained for the stent contraction tests conducted at the University of Michigan. From these results it becomes evident that repeating the experimental results with a dedicated stent fixture would lead to more reliable data points. Furthermore, repeating the experiment several times could also lead to more reliable data that affords opportunities to make significant conclusions. From comparison to figure 3.5, it becomes evident that less force is needed to shorten the stent longitudinally than is needed to elongate it in the reverse direction. It is likely that the stent design accounts for the location of implant, as it is more likely to be under contraction loadings rather than tensile in the popliteal segment. Thus, the stent must needs to contract more readily than it needs to elongate.

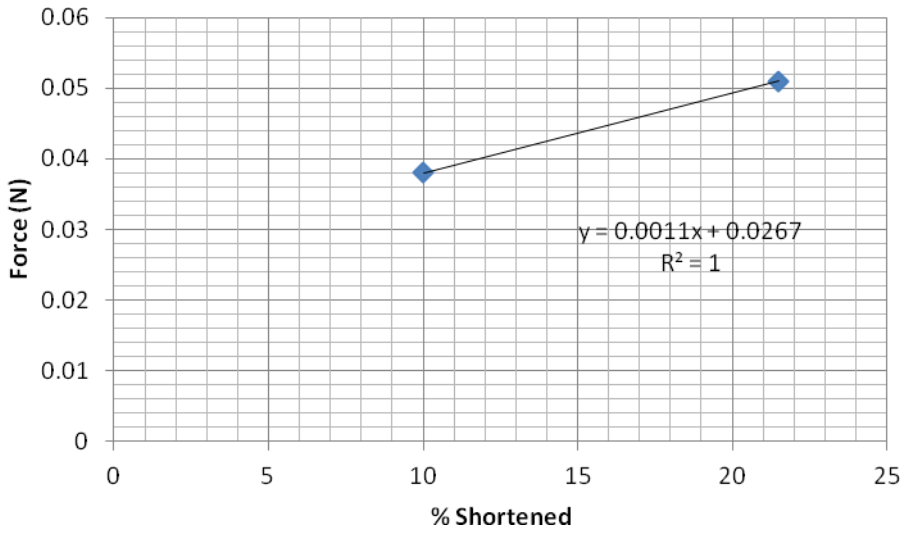

Figure 3.8: Contraction Test Results for Absolute Stent (U of M)

The crush test results from the University of Michigan study are shown in Fig. 3.9.

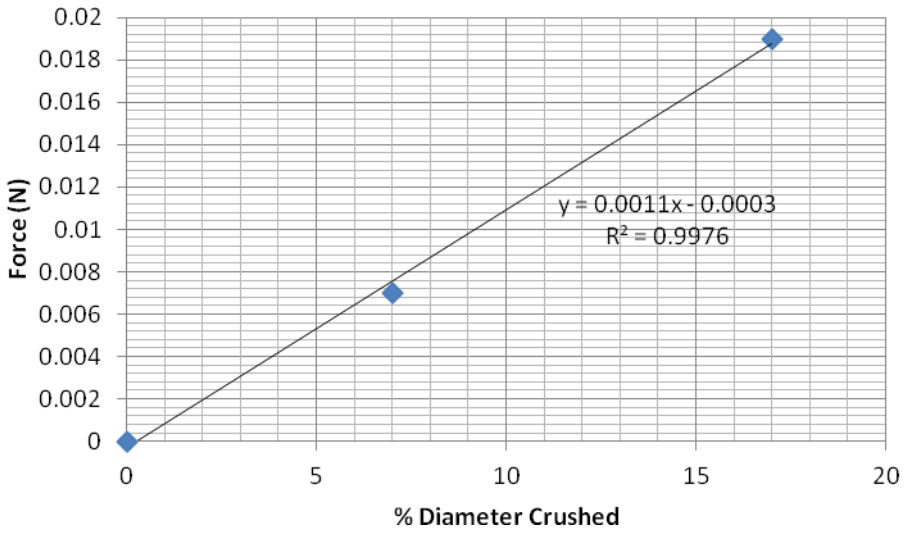

Figure 3.9: Crush Test for Absolute Stent (U of M)

From the crush test results it becomes that the absolute stent displays a linear relationship between the applied load and percent of stent diameter crushed. Compared to experimental values from Petrini et al. [2005] a similar linear relationship can be established, thus, validating the experimental procedure used at the U of M to determine the percent of the original diameter that is crushed when the stent is subjected to a forced loading. These experimentally determined values were compared to the theoretical crush tests carried out with FEM modeling using COMSOL.

No torsional experiments were carried out. However, the theoretical stent response to such a forced loading is also presented it in Chapter 2. An apparatus needs to be constructed to form a basis of comparison for these FEM results, and provide further validation of the theoretical model.

3.4. Conclusions

As expected, in the elastic tests a linear relationship exists between the applied load and the observed strain for the superelastic Nitinol stent specimen. The shortening/contraction results from both sets of experiments indicate that a linear relationship between the applied load and stent response.

For the tensile test to fracture the full load-strain curve was recorded. The results of this test showed the elastic region, the stent structure "transformation plateau," and the plastic deformation where the stent bridges broke. It was found that the stent could withstand large strains, more than 250% due to the stent structure and superelastic Nitinol properties. The load at which the first broken bridge occurred was determined to be 1.4 N, followed by two other breaks above 2 N. Moreover, the load at which the elastic region ends was determined to be approximately 0.8 N. The Absolute Nitinol stent can withstand tensile forces that are greater than those imposed on it *in vivo* due to the pulsatile loading by blood pressure, if one assumes a constant blood pressure of 100 mmHg or approximately 0.013 MPa.

CHAPTER 4: MODEL VALIDATION AND STENT GEOMETRY MODIFICATIONS

4.1 Introduction

In this chapter the theoretical results are compared to the experimental tensile test results to develop a correlation that may aid in the initial, pre-manufacturing attempts at designing novel stent geometries. One of the goals of this research is to improve the efficacy of the stent design process, by saving manufacturers time and resources. For this it is important for the theoretical and experimental data to be correlated. Good correspondence between the two data sets would allow manufacturers to easily eliminate poor stent geometry designs based on FEM simulations, and thus, eliminate the tendency to manufacture and test, and then re-manufacture, and re-test if the stent does not perform in the manner that was expected. Such an approach to stent design would exhaust resources and be time consuming. Thus, the theoretical data is compared to the experimental in a systematic manner that independently compares the load versus strain curves for each stent length, to the experimental data acquired for the actual Absolute stent.

In addition to the comparison of the theoretical and experimental data, four modifications were made to the Absolute stent geometry. These four stents were exposed to the same uniaxial loading conditions to determine the effect of the geometry changes. Based on the correspondence established between the theoretical and experimental data, it is likely that the modified stents will behave as predicted. The results are expected to yield trends from changes in the geometry that can be useful for future stent design.

4.2 Theoretical Data versus Experimental Data for Nitinol Absolute Stent

Comparison of theoretical data to experimental data was done to determine whether the static simulation results for the Absolute stent geometry are representative of the actual physical deformation. Successive iterations of the Nitinol material model became increasingly more detailed, are results from the FEM are presented along with the experimental data. Figure 4.1 shows the most basic Nitinol material model and its comparison to the experimental data.

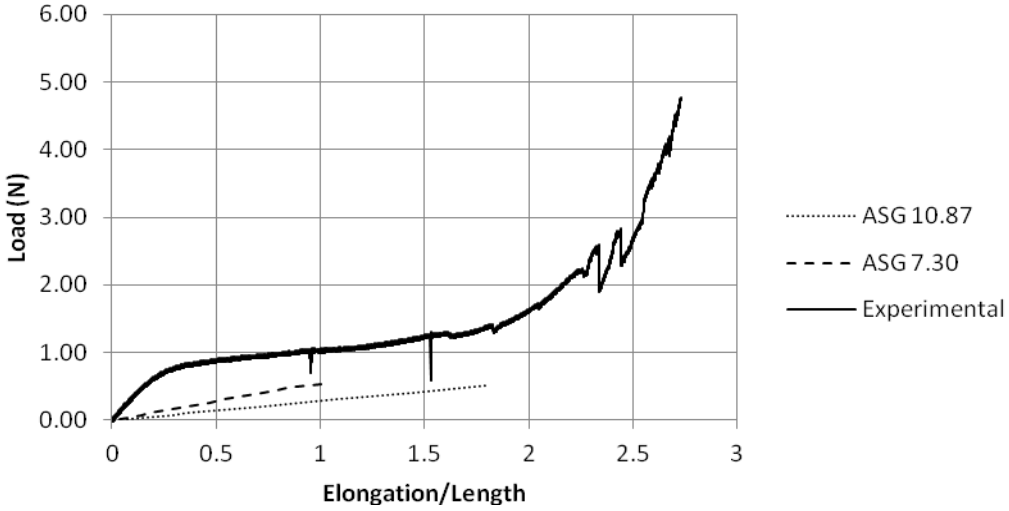

Figure 4.1. Experiment and Basic Nitinol Model

The theoretical data is not representative of the experimental data. Although both the experimental and theoretical have a linear elastic region, the slopes of these regions are visibly different. Figure 4.2 compares the three different stent lengths tested for the Absolute stent geometry against the experimental data. The nitinol material model for these three stent lengths was more complicated than the one previously used. For this material model, the transformation stress, and hardening function were specified. The value for the transformation stress was calculated based on the properties in Table 2.3, and a simplified relationship obtained by differentiating the Helmholtz thermodynamic potential with respect to the strain.

The experimental curve again has the highest sloped elastic region. For a more fruitful comparison, *only* the slopes of the elastic region for the theoretical and one experimental curves are compared in Fig. 4.3. In the plot the elastic region is steeper for the experimentally tested 105.44 mm stent. (Discuss the trend of the model results approaching the experimental results as the material model get more complicated.) This indicates that the longer stent is stiffer than the theoretically tested shorter stents. It would be interesting to experimentally test shorter lengths of the stent specimen to determine whether this pattern does in fact exist. It is likely that more bridges between individual struts, present in the actual stent, leads to steeper slope determined in this investigation.

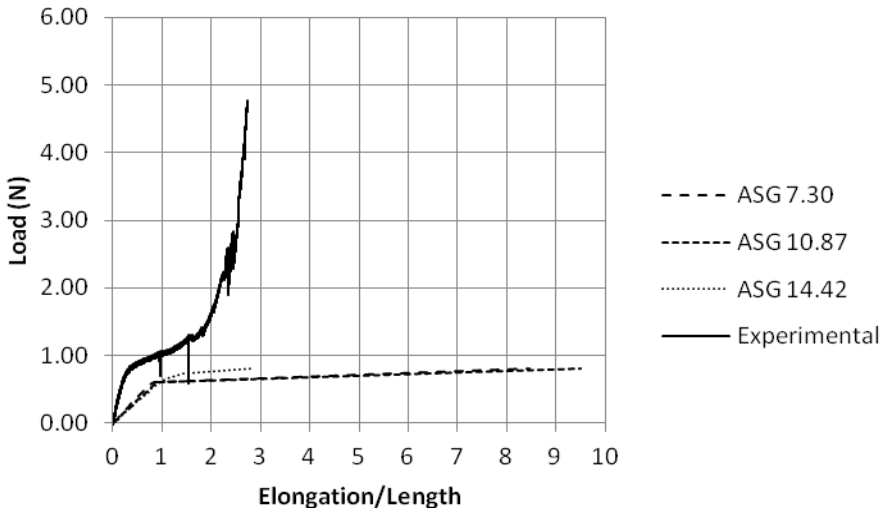

Fig. 4.2. Experimental Data compared to more complicated Nitinol model

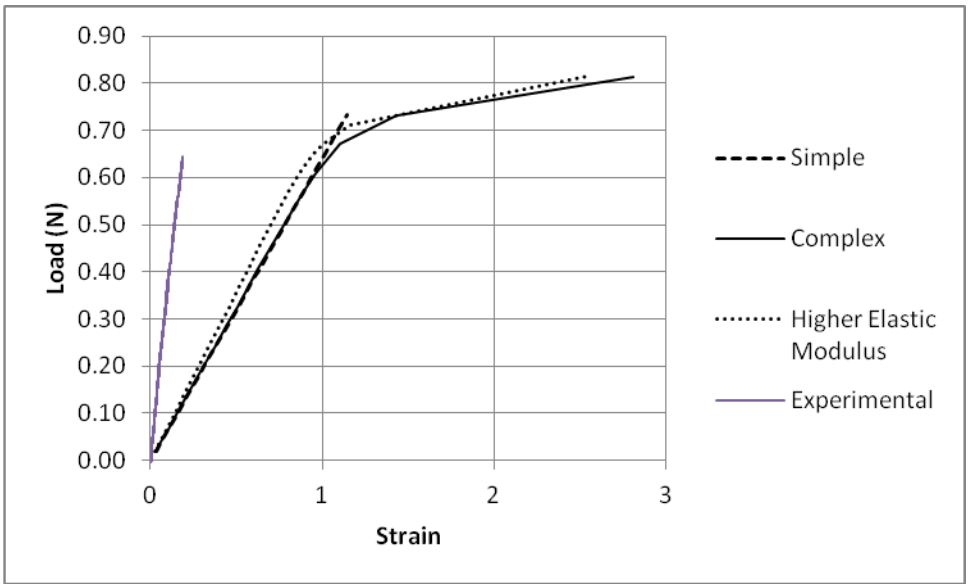

Fig. 4.3. Elastic region comparison between experimental and theoretical results

4.3 Proposed Design Changes

4.3.1 CAD Design

CAD drawings of the three modifications to the Absolute stent geometry were carried out in the same manner as the CAD rendering of the Absolute stent geometry. Figure 4.4 shows the CAD drawings of the different stent designs based on modifications to the Absolute stent geometry. These stent geometries were theoretically tested under several tension and compression loading scenarios.

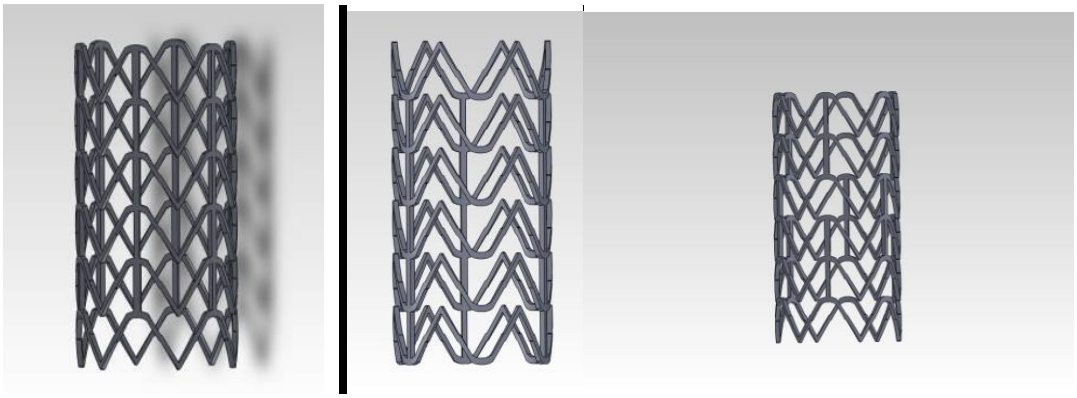

(a) **(b)** **(c)**

Fig. 4.4. (a) all link (MOD 1), (b) unstaggered (MOD 2), (c) Double Bridge Length (MOD 3)

In Fig. 4.4(a) bridges are added to link every endpoint on every strut in every row to the existing Absolute stent geometry. Whereas the original design alternates the connection point in each row, and staggers the first connection for alternating rows down the cylinder, this design fills in the points that are not connected in any row for the length of the stent. The modification in Fig. 4.4(b) is to simply un-stagger the starting point of the bridge elements so that the connection points alternate in every row, but are not staggered from row to row down the length of the stent. The resulting design is similar to the one in Fig. 4.4(a), except there are only three long connection columns, instead of six. Fig 4.4(c) is the same mesh layout as the Guidant Absolute stent, except the length of the bridges, which are doubled in length to 3.556 mm. The design in the bottom left elongates the bridge elements to twice the original length, and the modification in the bottom right alternates the bridges from the outside to the inside. These three modifications to the Absolute stent geometry were tested with the COMSOL Multiphysics software.

4.3.2 Theoretical Results for Modified Geometries

The theoretical results for the stents with the modified geometries are presented in comparison to the theoretical data for the actual Absolute stent geometry, and in comparison to the linear portion of the experimental load-displacement curve representative of the elastic region. Figure 4.6 shows load-strain plots for the 7.30 and 10.87 mm stents with the first modified geometry. In this modification bridges were added to every connection point, and as a result the number of bridges per row doubled from 3 to 6. Thus, for a 10.87 mm stent the total number of bridges increased from 15 to 30.

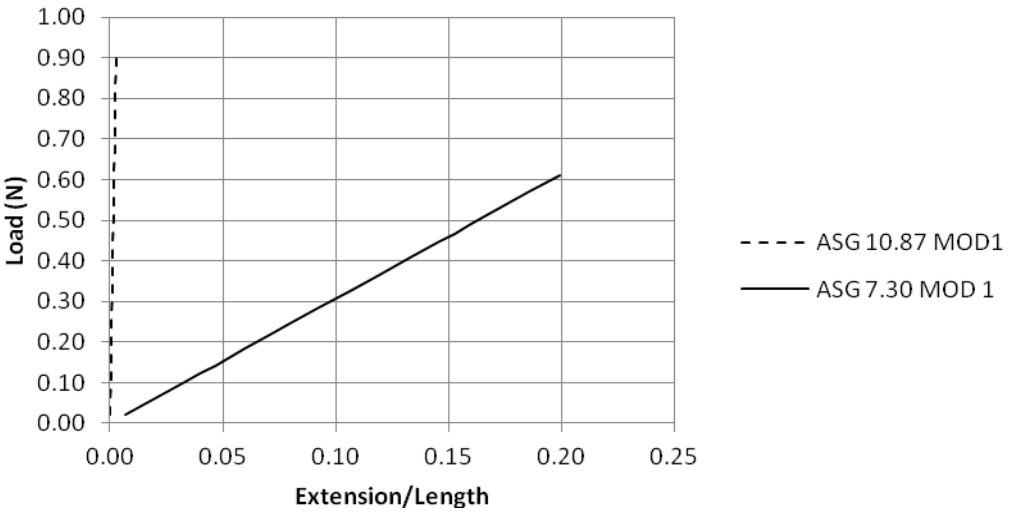

Fig. 4.5. Comparison of 7.30 and 10.87 mm stents with MOD 1

The results in Fig. 4.5 show the number of bridges between the strut elements significantly affect the rigidity of the stent structure. It should be obvious that a longer stent, by way of its length, has more total bridges, i.e., the 7.30 mm stent has 18 total bridges, compared to 30 for the 10.87 mm stent, and should be more rigid. This is demonstrated by the steeper slope for the 10.87 mm stent with this modification. Comparison of these two curves to the theoretical data for the actual Absolute stent geometry is shown in Fig. 4.6.

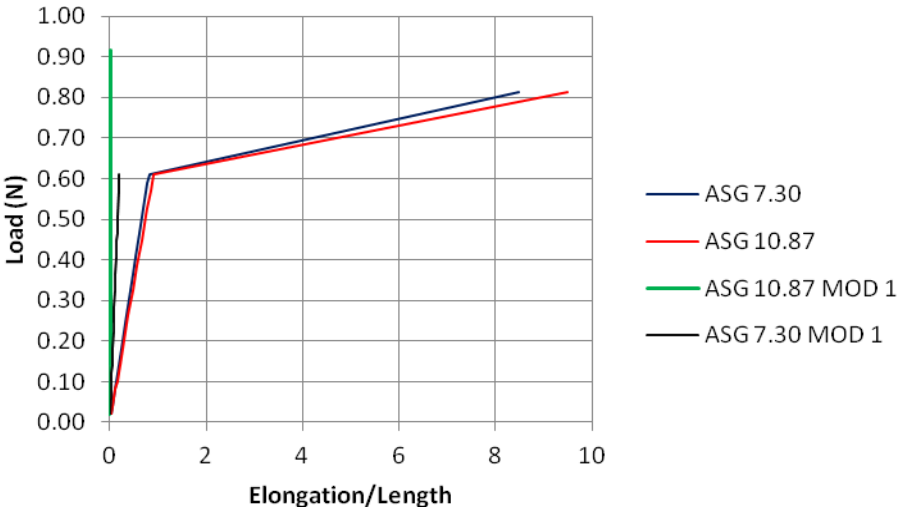

Figure 4.6: Comparison of Modified Stents to Actual Absolute Stent

The graph in Fig. 4.6 shows that adding bridge elements increases the rigidity of the overall stent structure. In fact, doubling the number of bridge elements present in the stent structure affects the slope of the elastic region more than increasing the length of the stent. This is

evidenced by the large discrepancy in the slopes of the modified 10.87 mm stent and the theoretical results for the actual Absolute stent geometry. It becomes evident that doubling the number of bridges from 15 to 30 increases the rigidity, and, thus, the slope of the elastic region for this stent structure.

Figure 4.7 shows the results for the 7.30 and 10.87 mm stent with the second modification. In this scenario the number of bridge elements was constant, but the location of the bridges was different from the actual Absolute stent geometry. The start of the bridges is staggered in the original stent design, but this is not the case for the second modification. The offset starting point of bridge elements from each row was adjusted so that each row had the same bridge locations. The linear elastic region is again well defined as it was in other simulation scenarios, and is used as a basis for comparison, as to the efficacy of these geometry modifications. From the plot in Fig. 4.7 it becomes evident that this design modification has an effect similar to that of the first design modification, in, which, the number of bridges for each stent length was doubled. The slopes of the elastic regions for the 7.30 and 10.87 mm stents with this modified geometry are indeed steeper than that predicted for the actual Absolute stent. Since the number of bridges was the same, perhaps the un-staggered configuration contributed to the increased stiffness and less uniaxial deformation for this stent geometry. Perhaps, the length of the bridge, which, in effect tripled due to the configuration, contributed to the increased stiffness of this stent geometry. The effect of doubling the length of the bridges while maintaining the bridge configuration of Absolute stent is investigated next.

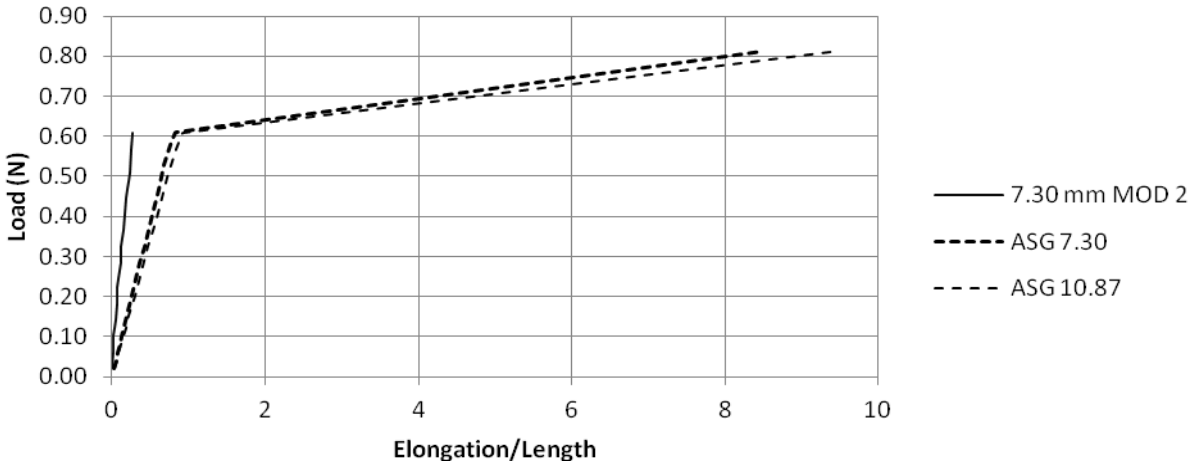

Figure 4.7: 7.30 and 10.87 mm stent with MOD 2

4.4. Conclusions

In this section two sets of comparisons were made: (1) experimental data was compared to the theoretical deformation data gathered in COMSOL, and (2) three geometry modifications to the Absolute stent were carried out and simulated for comparison to the simulations of the actual Absolute stent. The first was done in order to determine whether the modeling of stent deformation in COMSOL is possible. From the comparison of the experimental and theoretical data, the accuracy of the nitinol material model differs by. It was shown that as the material model increased in complexity, the load-strain results more closely resembled the experimental results. The FEM was able to adequately predict the load-strain behavior only in the first two stages of the curve. The model was not able to predict the stent behavior for large deformations, which is consistent with the literature for these types of studies. The discrepancy was attributed to the fact that the largest theoretically simulated stent was only approximately 15% of the length of the stent that was experimentally tested. Thus, the stiffness of the actual stent was attributed to the notion that there are more bridges in a longer stent.

The three modifications were tested to verify some of the observations from comparison to the experimental data. The first modification (MOD 1) doubled the number of bridges in the entire stent structure. From here it was discovered that the number of bridges has a more pronounced effect on the deformation of the stent when subject to an applied load, with more bridges leading to a more rigid stent structure. As such the linear elastic region of this modified geometry was much steeper than that predicted for the actual Absoulte stent. Modification 2 (MOD 2) simply changed the positioning of the bridges, by not staggering the starting position for alternating rows. In effect, this created one long bridge, and also increased the stiffness of the stent. Doubling the length of the bridges (MOD 3) led to.

Although the comparison of the experimental data to the theoretical data for the Absolute stent geometry is not a one-to-one correspondence the visual output from the COMSOL software indicates that it is possible to model stent behavior under forced loading conditions. The design modifications verify some intuitive ideas as to the stent geometry and how this contributes to the deformation behavior.

CHAPTER 5: CONCLUSIONS AND FUTURE WORK

5.1 Summary

Experimental and theoretical testing of the Guidant Absolute Nitinol stent was conducted in this study. In particular, tension, compression, and crush loads were applied to the actual stent under experimental conditions. The response and deformation of the stent were measured and recorded. The mechanical response of the SMA Stent structure was evaluated and then compared to the predicted deformation behavior of the stent to various static uniaxial tensile and compressive loading conditions. Due to the complications that arise with simulating contact forces, the crush test was not simulated in this study.

The theoretical solutions obtained in the COMSOL work environment utilized the structural mechanics branch of the software, and a series of expressions derived from the Helmholtz thermodynamic potential. These expressions defined the transformation stress, or the stress at which the Nitinol work material exhibits its characteristic phase change, and the hardening function. This was the most complicated material model defined for the Nitinol. Other less complicated material models that simply specified material parameters were also utilized. The modeling results were compared to the experimental results in order to determine whether the simulation results are representative of the actual physical deformation of the stent structure.

In addition to testing the Absolute stent geometry under these two different material models, there modifications to stent geometry were also tested under the more complicated material model. The three modifications tested included structural changes that specifically changed the bridge elements of the stent structure. The first modification doubled the number of bridge elements in the stent; the second changed the positioning of the bridge elements, and the third simply doubled the length of each existing bridge element. These geometry modifications were compared with the simulation results for the actual Absolute stent geometry.

5.2 Conclusions

In the experiments it was found that the load at which the elastic region starts to plateau is approximately 0.8 N. For smaller initial loadings the load-strain curve exhibits a linear elastic region, followed by a sloped plateau that represents the phase change from austenite to

martensite. At loads above this, large deformations were recorded, and particular adjustments of the stent geometry to accommodate the loading scenario were noticed. Specifically, the stent elongated so that the unconnected points of each strut alternated directions for the entire length of the stent. As the load was increased this alternating arrangement of stent elements became more pronounced. As the load is increased, the induced strain will linearly increase (elastic region) and then reach a plateau where small increases in the load lead to increased strain. This plateau is when the austenite to martensite phase change occurs. The load-strain curves indicate that the load at which transformation starts is approximately 0.8 N for the experimental case. Once this transformation is complete, increasing the load then leads to smaller increases in the strain, as the more rigid martensite phase is more prevalent. Finally, increasing the load led to breaks in the stent structure.

Most relevant conclusions in this study come from the comparison of the experimental and theoretical data, as well as from the comparison of the simulation of the modified stent geometries to the simulations of the actual stent geometry. It was shown that an adequate FEM could be constructed for modeling the stent behavior for small deformations. Although COMSOL is not specifically designed to handle large deformations, the different material models were able to predict the elastic region of deformation. The two different material models differ in their prediction of the slope of the elastic region. It was evident that the simplest material model predicted a slope for the elastic region that is visually very different from the experimentally determined elastic region. The more complicated Nitinol material model with plasticity and a forward transformation function defined improves on the simpler model, but still predicts the slope of the elastic region to be flatter than it actually is. The concentration of stress is not visible under the experimental uniaxial loading conditions. However, this is an advantage of using COMSOL. The von Mises stress distribution showed that the stress concentrated in the regions where the bridges connect to the next strut. In fact, it was evident from the stress concentration that one could expect these to be the regions where breaks in the structure would occur.

From the visual outputs from COMSOL it is evident that the stress concentrates near the connection point of a bridge to the next row of struts. In fact, the COMSOL software predicted that much of the stress would be distributed exactly, where the breaks first occurred under experimental conditions. Moreover, under uniaxial loading an interesting alternating pattern for

each strut was noticed for the length of the stent where the point of each triangle pointed in alternating directions. This same alignment pattern in response to the uniaxial tensile loading was also noticed in the simulation results. Regardless of length, the Absolute stent geometry simulation results indicate that the load at which transformation will occur is 0.7 N. This is a difference of 30%, which may be considered a large error. However, this would be more alarming if the simulation results predicted a transformation load that is more than what was experimentally determined.

Some interesting trends were noticed regarding the slope of the elastic region for the experimental and simulation results as well. The three simulated stent lengths with the absolute stent geometry indicate that increasing the length of the stent tends to make it less stiff, and lower the slope of the elastic region. However, the experimentally tested stent, which is longer than all three simulated stents, exhibits an elastic region slope that is steeper than any simulation curves. This discrepancy can be explained if one realizes that it is not the length of the stent that contributes to it stiffness; rather it is the number, position, and length of the bridges in the stent. Intuitively, more bridges would lead to increased stiffness, and this was the case as the total bridges are far larger in a 100 mm stent compared to a 7.30 mm stent.

An attempt was made to verify this dependence on the bridge number, position, and length by modifying the Absolute stent geometry to reflect these scenarios. MOD 1 doubled the number of bridges in the stent geometry, MOD 2 rearranges the location of the bridges, and MOD 3 doubled the length of the bridges, while maintaining their positions. From MOD 1, it was determined that the number of bridges does in fact have a more pronounced effect on the stiffness of the stent. As such, for the same loads less elongation/contraction was noticed, and the resultant elastic regions were indicated by lines with slopes steeper than any length of the actual stent geometry simulated. MOD 2 had a similar effect as rearrangement, in effect, created a stent with three bridges that ran the length of the stent.

5.3 Contributions

Specific contributions of this study are twofold: (1) methodology and (2) classification:

(1) This study sets the foundation for a tool that can predict behavior of new and existing Nitinol stent designs. The methodological contributions stem from the fact that stent design and manufacture is a resource intensive operation. In this study the techniques of CAD and FEM

were developed in moving toward a more robust mode of stent design. The groundwork has been laid here, as the mechanical testing of stent geometries has been shown to be possible in the COMSOL environment.

(2) The classification of the Guidant Absolute stent is another contribution of this study. Currently there are no significant efforts to database the mechanical properties of different stent structures. This study contributes the theoretical mechanical response of the absolute stent and three modified stents to various forced loading conditions. By keying exclusively on the mechanical response, the initial phases of stent manufacture may be improved by allowing researchers and professionals an opportunity to visualize their design's response to forced uniaxial loading conditions. If a stent geometry can show similar experimental and theoretical results as is shown here, it is suggested that a theoretical design tool for stenting is possible.

5.4 Future Work

This study focuses only on the mechanical response of the stent to forced loading conditions and is limited by the commercial COMSOL code. Since stents are implantable devices, a more relevant study would examine the stent not only to stationary forced loading conditions, but to the more dynamic loading conditions experienced within the body. Future studies should include interactions between the stent and the arterial wall, in addition to any pulsatile loading conditions that would result due to blood pressure. Although researchers have attempted to address these issues for other stent geometries made of medical grade steel, the behavior of the stent to loading conditions with contact forces is a far more challenging problem that has not been completely explored.

In addition to more complicated loading and contact scenarios, future studies should include a more complicated material model for Nitinol. Although the Helmholtz potential was used to define certain material parameters in the COMSOL work environment, solution of this equation simultaneously with the structural mechanics branch was not successfully carried out. This might account for some of the inconsistencies in the acquired data. Moreover, other hardening models as suggested by Lagoudas [2008] can be tried out.

References

Annual Book of ASTM Standards, Section 13: Medical Devices and Services. Volume 13.01: Medical and Surgical Materials and Devices; Anesthetic and Respiratory Equipment; Manufacture of Pharmaceutical Products. ASTM International, 2009.

Brand, M., Ryvkin, M., Einav, S., Slepyan, L., "The Cardicoil Stent-Artery Interaction." Journal of Biomechanical Engineering. Vol. 127 April 2005.

Chua, David S.N., Mac Donald, B.J., Hashmi, M.S.J., "Finite Element Simulation of Stent Expansion." Journal of Material Processing Technology 120 (2002) 335-340

Collet, M. "Modeling Implementation of Smart Materials such as Shape Memory Alloys and Elctro-Active Metamaterials. Excerpts from the Proceedings of the COMSOL Conference 2008. Hannover.

COMSOL Reference Manual v 3.3

COMSOL Reference Manual v 4.2a

Conti, M., "A Finite Element Analysis of Self-Expanding Braided Wirestent." A Thesis Submitted to Ghent University. 2007.

Duerig, T.W., Wholey, M. "A Comparison of Balloon- and Self-Expanding Stents." Min Invas Ther & Allied Technol 2002: 11(4) 173-178.

Duerig, T.W., Melton, K.N., and Wayman, C.M. "Engineering Aspects of Shape Memory Alloys." Boston: Butterworth Heinemann, 1990.

Duerig, T.W., Tolomeo, D.E., and Wholey, M. "An Overview of Superelastic Stent Design." Min Invas Ther & Allied Technol. 2000. 9 (3/4) 235-246.

Duda, S., Wiskerchen, J., Tepe, G., Bitzer, M., Kaulich, T.W., Stoeckel, D., Claussen, C., "Physical Properties of Endovascular Stents: An Experimental Comparison." JVIR 2000; 645-654.

Early, M., Kelly, D.J., "The Role of Vessel Geometry and Material Properties on the Mechanics of Stenting in the Coronary and Peripheral Arteries." Journal of Engineering in Medicine. 2010. Vol. 224 Part H: 465-473.

Eaton-Evans, J., Dulieu-Barton, J.M., Little, E.G., Brown, I.A., "Thermoelastic Studies on Nitinol Stents." Journal of Strain Analysis. Vol. 41 No. 7. I MechE 2006.

Ghosh, P, DasGupta, K., nag, D., Chanda, A. "Numerical Study on Mechanical Properties of

Stents with Different Materials During Stent Deployment with Balloon Expansion." Excerpts from the Proceedings of the 2011 COMSOL Conference. Bangalore.

Lagoudas, D.C., "Shape Memory Alloys: Modeling and Engineering Applications." Springer, 2008.

Lally, C., Dolan, F., Prendergast, P.J., "Cardivascular Stent Design and Vessel Stresses: A Finite Element Analysis." Journal of Biomechanics 38 (2005) 1574-1581

Liang, D.K., Yang, D.Z., Qi, M., Wang, W.Q., "Finite Element Analysis of the Implantation of a Balloon-Expandable Stent in a Stenosed Artery." International Journal of Cardiology 104 (2005) 314-318

Lin, Z., Pike, K., Zipse, A., Schlun, M. "Investigation on Stent-Finish specimens using Tension-Tension Method." Journal of Materials Engineering and Performance. Vol 20(4-5) 2011.

Lubarda, V.A. "On Thermodynamic Potentials in Linear Thermoelasticity." International Journal of Solids and Structures. 41 (2004) 7377-7398

Ma, D. "A New Stent Design for the Femoropopliteal Segment." ME 590 Report. University of Michigan. 2006

McGarry, J.P., O'Donnell, B.P., McHugh, P.E., McGarry, J.G. "Analysis of the Mechanical Performance of a Cardiovascular Stent Design based on Micromechanical Modelling." Computational Materials Science 31 (2004) 421-438

Melzer, A., Stoeckel, D. "Function and Performance of Nitinol Vascular Implants." The Open Medical Devices Journal. 2010, 21 32-41

Migiliavacca, F., Petrini, L., Massarotti, P., Schievano, S., Auricchio, F., Dubini, G., "Stainless and Shape Memory Alloy Coronary Stents: A Computational Study on the Interaction with the Vascular Wall. Biomechanical Model Mechanobiol 2 (2004) 205-217.

Migiliavacca, F., Petrini, L., Montanari, V., Quagliana, I., "A Predictive Study of the Mechanical Behavior of Coronary Stents by Computer Modeling." Medical Engineering & Physics 27 (2005) 13-18

Migiliavacca, F., Petrini, L., Colombo, M., Auricchio, F., "Mechanical Behavior of Coronary Stents Investigated through the Finite Element Method." Journal of Biomechanics 35 (2002) 803-811

Mori, K., Saito, T. "Effect of Stent Structure on Stent Flexibility Measurements." Annals of Biomedical Engineering, Vol. 33, No. 6, June 2005: 733-742

Pelton, A.R., Duerig, T.W., "Nitinol Medical Devices," Advanced Materials and Processes. October 2005.

Pelton, A.R., Duerig, T.W., Stockel, D., "A Guide to Shape Memory and Superelasticity in Nitinol Medical Devices." Min Invas Ther & Allied Technol 2004: 13(4) 218-221

Petrini, L., Migliavacca, F., Massarotti, P., Schievano, S., Dubini, G., Auricchio, F., "Computational Studies of Shape Memory Alloy Behavior in Biomedical Applications." Journal of Biomechanical Engineering. 2005.

Petrini, L., Migliavacca, F., Auricchio, F., Dubini, G., "Numerical Investigation of the Intravascular Coronary Stent Flexibility." Journal of Biomechanics 37 (2004) 495-501.

Shrivastava, S. "Simulation for Thermomechanical Behavior of Shape Memory Alloy (SMA) using COMSOL Multiphysics. Excerpt from the Proceedings of the COMSOL Conference 2006. Bangalore.

Simons, J.W., Dalal, A., Shockey, D.A., "Load Deformation Behavior of Nitinol Stents." Experimental Mechanics. 2010: 50: 835-843.

Spencer, A.J.M., "Continuum Mechanics." Longman Group Limited. 1980.

Stoeckel, D., Bonsignore, C., Duda, S., "A Survey of Stent Designs." Min Invas Ther & Allied Technol. 2002: 11(4) 137-147

Stoeckel, D., Pelton, A., Duerig, T. "Self Expanding Nitinol Stents: Material and Design Considerations." Eur Radiol. 2004: 14: 292-301.

Stolpmann, J., Brauer, H., Stracke, H.J., Erbel, R, and Fischer, A. "Practicability and Limitations of Finite Element Simulation of the Dilation Behavior of Coronary Stents." Mat.-wiss.u.Werkstofftech. 34, 736-745 (2003).

Wang, R., Chandar, R.K. "Mechanical Response of a Metallic Aortic Stent—Part II: A Beam-on-Elastic Foundation Model. Journal of Applied Mechanics Vol 71. September 2004.

Wang, Wei-Qiang, Liang, D., Yang, D, Qi, M., "Analysis of the Transient Expansion Behavior and Design Optimization of Coronary Stents by Finite Element Method." Journal of Biomechanics 39 (2006) 21-32